Franziska Temme, Thomas Mölg, Jenny Turton und Tobias Sauter

Föhn events in Southern Patagonia

Climatological characteristics and process-based modelling

Mountain chains have an important impact on the regional climatic and weather conditions by shaping the large-scale flow. A typical phenomenon occurring in the lee of mountain chains are föhn events. With the Andes' orientation perpendicular to the prevalent westerly flow, Patagonia is predestined for föhn winds. Those events can influence various fields like climatology, glaciology and biogeography. The present study provides a first föhn climatology and gives an overview of mesoscale processes involved. Observational data from four Automatic Weather Stations (AWSs) distributed in west-east direction across the Andes at around 51 °S is used for the detection of föhn events. By high-resolution (1 km) atmospheric modelling with the Weather Research and Forecasting (WRF) model, one case study event can be analysed regarding the involved mesoscale processes at the study site and over a larger area (48 °S – 52 °S, 75.5 °W – 72 °W) including the Southern Patagonian Icefield (SPI). Results deliver a frequency of at least 87 events over the study period of one year (June 2018 – May 2019) with higher föhn activity during spring and summer. The case study event is forced by strong north-westerly flow. Stable air masses of high velocity encountering the Andes cause intense vertical air motion in the lee, e.g. mountain waves. The flow regime can be classified as non-linear, being reflected in phenomena like a downward windstorm and the formation of a hydraulic jump. It is shown that the case study event expands over major parts of the SPI with similar characteristics. Considering the high frequency of föhn events, a significant impact on the local climate is evident.

Keywords: **Patagonia, Föhn, WRF, numerical modelling, atmospheric processes**

1 Introduction

Mountain chains play a crucial role for the regional weather and climate. On one hand, the local weather conditions respond to the large-scale flow and mountain interaction. On the other hand, they affect the large-scale circulation on the synoptic and planetary scale (Schär 2002: 29). The Andes are an especially prominent obstacle due to their length, height and continuity and because they are the most significant mountain range in the Southern Hemisphere. This disruption of the atmospheric circulation with strongly prevailing westerly air flow results in various phenomena and an extreme west-east precipitation gradient (Garreaud 2009: 1). One important phenomenon is a warm, dry downslope wind, known as föhn wind. The perpendicular orientation of the Andes towards the mainly prevailing westerly flow favours the generation of föhn winds east of the Andes (Garreaud 2009: 7).

Patagonia holds the largest glaciated area in the Southern Hemisphere outside Antarctica (Rignot et al. 2003: 434) with glaciers largely contributing to sea-level rise (Braun et al. 2019: 130ff.). Glacier mass budgets, however, contain high uncertainty because precipitation amounts can still not be accurately estimated (Weidemann et al. 2018b: 14) and a meteorological network with sufficient spatial density and record length is missing due to the remote location and difficult accessibility (Garreaud et al. 2013: 217). The influence of föhn winds on glacier surface energy balances has been demonstrated in several studies worldwide (e.g. King et al. 2017; Turton 2017; Elvidge et al. 2020). Föhn events are associated with, on the one hand, increased precipitation, yet on the other hand, with enhanced ablation (Schneider et al. 2003; Speirs et al. 2010; Turton et al. 2018; Wiesenekker et al. 2018)

Föhn research has for a long time been limited to areas in the northern hemisphere, like the European Alps that are, subsequently, most well studied (Turton 2017). In the Southern Hemisphere föhn winds are still poorly investigated. Over the Southern Patagonian Icefield, no study about föhn has been conducted before.

In this study, the number, extension and the mesoscale flow patterns of föhn winds in southern Patagonia are examined. The study site is located on the southern edge of the Southern Patagonian Icefield (SPI) around 51°S, where four Automatic Weather Stations (AWSs) are situated. This observational data is used for detection of föhn events over a one-year period from June 2018 to May 2019. This analysis reveals information about the frequency of föhn events at the study site. Furthermore, one case study föhn event (08 August 2018 to 09 August 2018)

is identified, which is further analysed regarding the mesoscale flow by a high-resolution atmospheric model. The simulation is performed using the Weather Research and Forecasting (WRF) (Skamarock et al. 2019) model. The mesoscale analysis reveals information about the synoptic situation inducing föhn events, characteristics of the upstream air masses, flow patterns while overcoming the Andean chain, and phenomena in the lee caused by the föhn flow.

2 State of the art and aims of the study

2.1 Historical föhn research

Studying föhn effects started in the European Alps, where the warm, dry downwind got its generic name "föhn". The traditional definition describes föhn as a "wind warmed and dried by descent, in general on the lee side of a mountain" (*World Meteorological Organization* 1992: 246). Later on, research expanded to other locations in the Northern Hemisphere, like the Rocky Mountains in North America or to the Mediterranean Sea (e.g. Gohm et al. 2008). In the Southern Hemisphere, föhn is studied in New Zealand and in the Antarctic Peninsula (e.g. Speirs et al. 2010; Cape et al. 2015; Turton et al. 2018). In South America, föhn winds are poorly investigated, focusing on the higher populated regions in Argentina (30°S – 40°S) (e.g. Seluchi et al. 2003; Norte et al. 2008; Garreaud 2009; Norte 2015). In southern Patagonia, föhn is poorly studied for various reasons: In climate models, those events are difficult to represent due to the complexity of the orography. Furthermore, Patagonia lacks a meteorological network with sufficient spatial density and record length due to its remote location and difficult accessibility (Garreaud et al. 2013: 217). Different studies investigated the interaction of the Andes with large-scale circulation and precipitation amounts in southern Patagonia and, thereby, touched on possible föhn events (e.g. Smith/Evans 2007; Garreaud et al. 2013; Lenaerts et al. 2014; Viale and Garreaud 2015). Other studies focus on the Patagonian icefields and their mass balances where föhn events have an impact on accumulation as well as ablation (e.g. Weidemann et al. 2018a; Villarroel et al. 2013). Thus, in all these studies, föhn winds are not the research focus, but a factor that needs to be considered and is difficult to estimate because it is still poorly investigated.

2.2 Föhn processes

Föhn events are typically characterized by a lee-side increase in air temperature, decrease in relative humidity and increase in wind speed (Turton et al. 2017: 193). In Patagonia, intense upslope rainfalls and rain shadow effects east of the mountains are associated with orographically induced uplift (Garreaud et al. 2013: 215f.). The two most well-known föhn mechanisms (Figure 1) are briefly outlined:

During isentropic drawdown (Figure 1a), the low-level flow is blocked by the mountain and prevented from ascending. Thus, upper air, that is potentially warmer and drier in stable atmospheres, is advected isentropically upwind of the mountain barrier and subsides down the lee slopes (Richner/Hächler 2012: 222). The descending air mass warms at the dry adiabatic lapse rate. In reality this mechanism is seen as more important, however, the second thermodynamic mechanism is more well-known (Elvidge/Renfrew 2016: 456).

In thermodynamic föhn theory (Figure 1b), low-level airflow is strong enough to ascend the windward side of the obstacle. It initially cools at the dry adiabatic lapse rate until reaching saturation forcing condensation and precipitation. Afterwards, it rises cooling at the saturated adiabatic lapse rate.

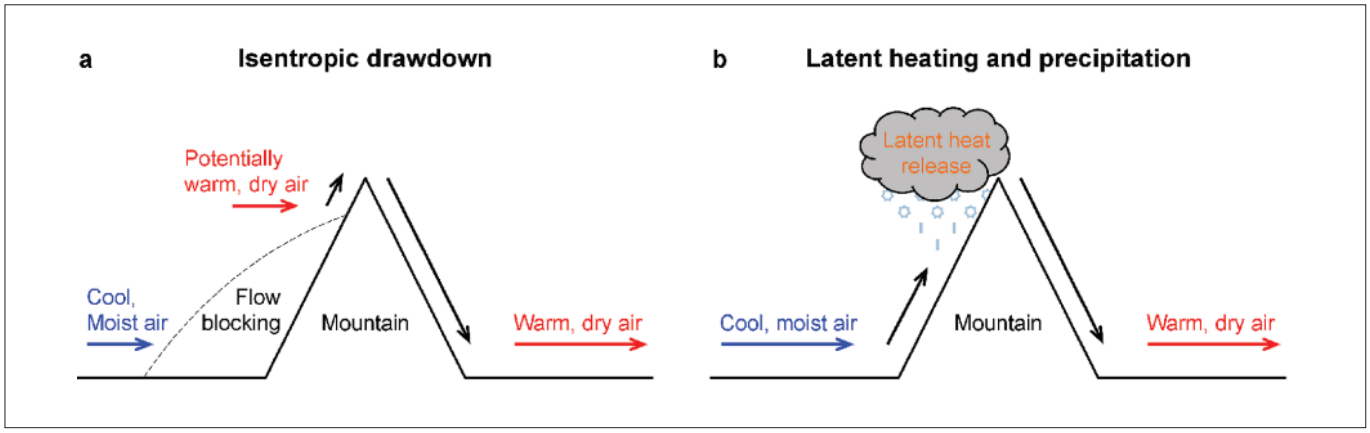

Fig. 1: Föhn warming mechanisms (Elvidge/Renfrew 2016: 457)

When the mountain has been overcome, moisture has been removed from the air, hence it descends warming at the dry adiabatic lapse rate. Consequently, the air in the lee is adiabatically warmer and drier than air at the same altitude on the windward side (Richner/Hächler 2012: 220ff.).

When stably stratified air is forced over a topographic obstacle, as during föhn flow, atmospheric disturbances form downstream, mostly acting on the mesoscale (Lin 2007: 109ff.). The most important observations during föhn events are lee waves, the formation of rotors and clouds in the lee, hydraulic jumps and the formation of jets through mountain gaps.

For approaching air that has sufficient inertia to overcome stability and cross the mountain barrier, vertical displacement can occur according to linear theory. The vertical displacement leads to the formation of gravity waves that oscillate around their equilibrium level at the so-called Brunt-Väisälä frequency N (Stull 1988: 601). Gravity waves forced by mountains are called mountain waves. Those can cause several flow dynamics like lee windstorms or clear-air turbulence. Furthermore, the waves carry momentum and energy into the stratosphere when vertically propagating and, thus, can also impact the larger-scale circulation (Jackson et al. 2013: 122ff.).

The flow over a mountain can also be considered as a shallow water flow, which can be described by the hydraulic theory. The flow regime can be divided into "subcritical", "critical" and "supercritical" by the Froude number Fr. If the upstream flow has enough kinetic energy to overcome the potential energy barrier of the obstacle, the flow regime is supercritical. If the perturbation flow converts its potential energy into kinetic to gain enough energy to overcome the obstacle, the flow regime is subcritical (Kirshbaum et al. 2018: 13f.). When subcritical flow changes to supercritical flow at the top of the obstacle, strong downward acceleration in the lee occurs. In some cases, the air adjusts to the downstream conditions in a hydraulic jump (Durran 1990: 66ff.).

2.3 Aims of the study

This study investigates the frequency and mesoscale flow of föhn events in southern Patagonia. Föhn events impact many different fields influencing forest fire activity (e.g. Mofidi et al. 2015) or glaciers: They can affect ablation through rising temperatures and increased solar radiation and wind velocities, and accumulation through precipitation on the windward slopes (Schneider et al. 2003; Speirs et al. 2010; Turton et al. 2018; Wiesenekker et al. 2018). This study can improve the understanding of glacier behaviour in southern Patagonia and the regional understanding of föhn events, since the föhn patterns in southern Patagonia have not been investigated so far.

The two main aims of this study are:

a) *Identification of föhn events:*
   The frequency and spatial extent of föhn events in southern Patagonia are not known. For the detection of föhn events, a Föhn Identification Algorithm is developed based on AWS measurements. With this algorithm, the frequency of föhn events is determined over the study period of one year.
b) *What are the mesoscale processes during a föhn event, and how representative are those processes at the study site for the Southern Patagonian Icefield?*
   The physical mechanisms controlling föhn events and the typical flow patterns are investigated at the study site using WRF. Additionally, it is analysed if the case study event extends over the whole SPI.

In order to answer these research questions, the study is structured as follows: Section 3 gives an overview of the geography and climatic situation at the study site. In section 4, the observational and gridded datasets are described as well as the methods used to process those. Furthermore, the methodologies are presented. Section 5 provides the results of the study including the results of the föhn detection, the evaluation of the WRF model output and the results of the high-resolution mesoscale analysis (5.3). Furthermore, the spatial extent of the case study event is analysed, and it is investigated if the study site represents föhn conditions over a larger area (5.4). Finally, section 6 presents the main findings of the study.

3 Study site

With Patagonia (40°S – 55°S), South America holds the only continental land mass south of 48°S. This makes the region very important as a place of study for the climatic conditions of the Southern Hemisphere's higher midlatitudes. The atmospheric circulation is disrupted by the Andean chain that, at these latitudes, rises to about 1500 m in the mean with peaks reaching above 3000 m (Garreaud 2009: 1). Due to the complex topography, the region is poorly resolved in low-resolution general circulation models and reanalysis models (Lenaerts et al. 2014: 4608).

The Patagonian icefields are the largest glaciated area in the Southern Hemisphere outside Antarctica (Rignot et al. 2003: 434), covering a total area of 17,900 km^2. The Southern Patagonian Icefield is the biggest glaciated region of the Andes with an area of 12,232 km^2 (Braun et al. 2019). Recent studies have shown that the glaciers are retreating rapidly.

Due to their potential contribution to sea level rise and their strong sensitivity to climate variations, it is important to further investigate the glacier behaviour in Patagonia (Bravo et al. 2019: 2f.). One challenge for glaciological studies is the high uncertainty in mass balance models, especially concerning the accumulation. Surface mass balance studies found an increase in ice mass at the surface in recent years (Schaefer et al. 2013, Mernild et al. 2017), which contrasts with the observed shrinkage. However, as accumulation is highly depending on the amount of solid precipitation, climate mass balance models are affected by considerable uncertainties depending on the precipitation modelling scheme. This leads to high differences for example in climatic mass balance results and glacier contribution to sea level rise (Weidemann et al. 2018b: 14; Sauter 2020: 2). Therefore, it is important to provide further knowledge on the processes affecting glacier behaviour, such as föhn events.

This study provides investigations on two scales concerning the study area. The main focus lies on a region in the southern part of the SPI, between Glacier Amalia and Glacier Grey, where the AWSs are situated (Figure 2), referred to as the 'study site'. Additionally, a wider study area (48°S – 52°S, 75.5°W – 72°W) including the whole SPI is investigated using the WRF model output. Thus, the föhn flow patterns are not only examined in the AWSs' environments, but also on a larger region. It can be shown, how föhn flow is modified from the Pacific Ocean until far into the lee. Furthermore, it is investigated if föhn builds simultaneously over wider areas of the SPI, and which areas are affected.

Patagonia is situated between the circumpolar low-pressure band around Antarctica at about 60°S and the high-pressure ridge in the South Pacific around 30°S. This generates a strong and constant upper-air westerly jetstream (Lenaerts et al. 2014: 4611). The westerly winds are embedded in the circumpolar storm track (on average between 40°S and 50°S). The westerly flow prevails year round, although the maximum shifts with the storm track from between 45°S and 55°S in summer to between 35°S and 45°S in winter (Garreaud 2009: 2ff.). The local climate is highly influenced by the mountainous terrain and the glaciers on site. Highest temperatures are measured in December to February (austral summer) as well as highest precipitation amounts which can be

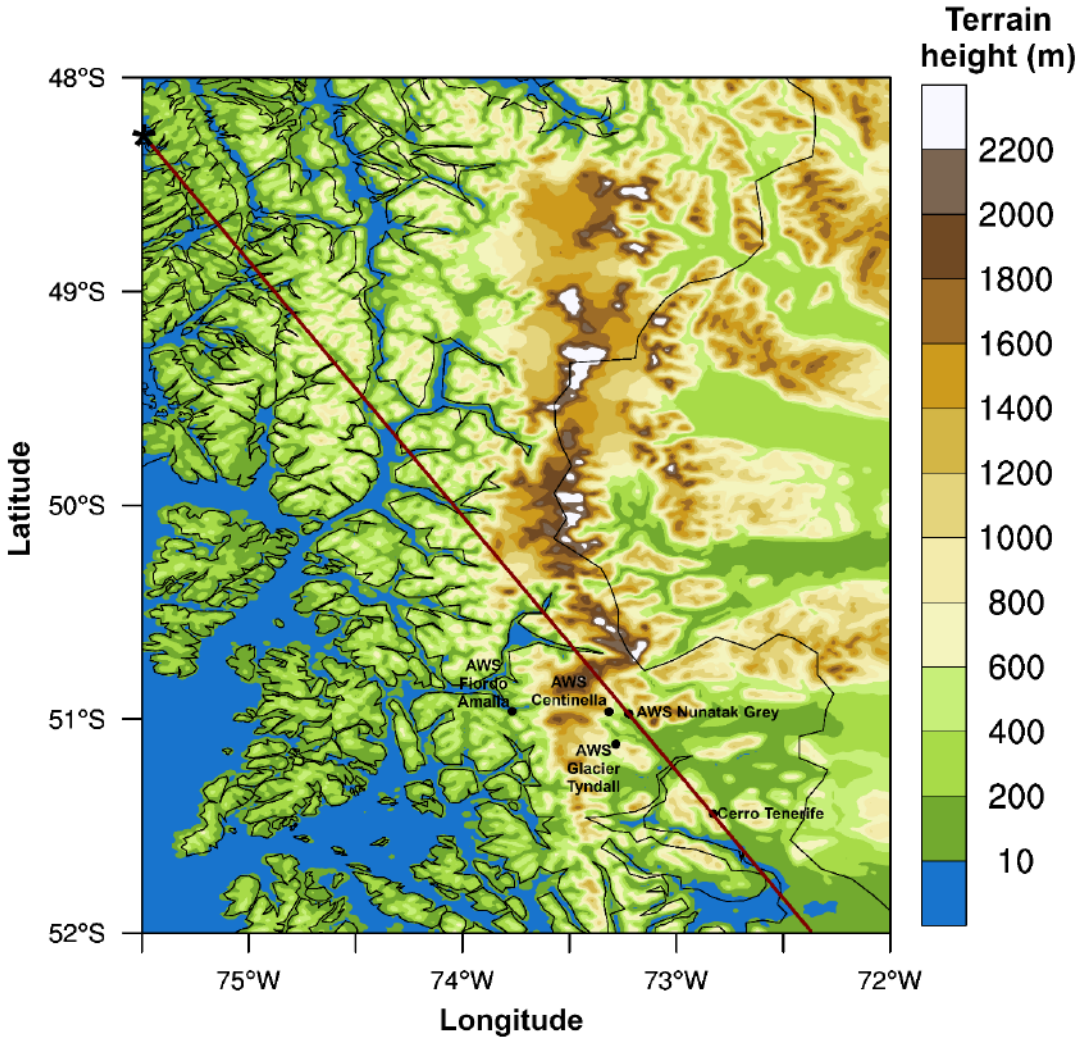

Fig. 2: Topographic overview of the study site. The outer framework reflects the wider area used for the analysis of WRF output including the Southern Patagonian Icefield. Black dots mark the four AWSs in the main study site and the station at Cerro Tenerife. Red line displays the course of the cross sections. The black star in the top left corner marks the location where the upstream flow is investigated. Black lines are the country outlines.

attributed to the higher cyclonic activity on site due to the southward shifting of the westerly wind belt.

The Andes are oriented perpendicular to the main flow. Consequently, wet air masses from the west are blocked and rise over the windward side of the Andes generating abundant precipitation. East of the mountains, rain shadow effects prevent rainfall with dry downwinds blowing from the mountains. This generates an extreme precipitation gradient between the western and eastern side of the Andes (Garreaud et al. 2013: 215f.). Sauter 2020 reports average precipitation amounts of about 5060 mm to 5990 mm per year for the SPI with absolute maxima of 10,090 mm to 11,580 mm per year. These values are considerably lower than estimates of previous numerical studies (e.g. Lenaerts et al. 2014; Schaefer et al. 2015).

4 Data and Methods

4.1 AWS Data

In this study, data of four Automatic Weather Stations is used with locations shown in Figure 2. In Table 1, the stations are listed. Additionally, air pressure and temperature measurements of AWS Cerro Tenerife (51°26′31.7″S, 72°49′37.5″W) were used.

AWS Fiordo Amalia (FA) (45 m a.s.l.) represents the conditions on the windward side. Values measured are air temperature *T*, relative humidity *RH* and precipitation *R* in daily and hourly resolution, respectively. The operating institution is the Chilean Water Directorate (Dirección General de Aguas; DGA) of the Ministry of Public Works.

AWS Centinella (CE) (1100 m a.s.l.) represents the atmospheric conditions at the eastern side of the mountain plateau. Variables measured are *T*, *RH*, *R*, global radiation *G*, wind speed *U* and wind direction *Dir* in hourly resolution. Due to the exposure to extreme winds, the wind sensor broke during a strong wind event. The station was installed for a project of the German Research Foundation, and has afterwards been maintained by Dr. Tobias Sauter of the Climate System Research Group at Friedrich-Alexander-Universität Erlangen-Nürnberg. The sensors and the accuracies given by the producer are listed in Table 2. The precipitation uncertainty needs to be increased due to the extreme wind speeds that AWSs are subjected to in the mountainous terrain of Patagonia. As the tipping-gauge rain buckets, that are used for precipitation measurements, are usually unshielded, rainfall is often underestimated during situations with high wind speeds because of deformation of the wind field. However, through vibration of the gauge it may also be overestimated. Additionally, snowfall cannot be measured with the sensor because the instrument is not heated (Schneider et al. 2003: 108f.). Overall, an additional uncertainty of 50% is estimated (Sauter, pers. comm.).

AWS Nunatak Grey (NG) (320 m a.s.l.) is located on rock at the nunatak of Glacier Grey representing the föhn conditions in the lee. Measurements comprise 10-minute intervals of *T*, *RH*, *G*, *U*, *Dir* and *R*. The station is operated by the climate geography group at the Humboldt-University Berlin. The sensors used are the same as for CE. Thus, precipitation measurements face the same wind-based error-proneness. The three

Tab. 1: AWSs and their locations, measured variables (air temperature T, relative humidity RH, global (total incoming shortwave) radiation G, wind speed U, wind direction Dir and precipitation R) and recording times (after Temme et al. 2020).

AWS	Altitude	Location	Variables	Available data since	Temporal resolution
FA (windward)	45 m	50°57′44.7″S, 73°46′06.2″W	T, RH, R	2015	Daily, hourly
CE (mountain)	1100 m	50°57′54.5″S, 73°18′54.0″W	T, RH, G, U, Dir, R	2017	Hourly
NG (lee)	230 m	50°58′32.0″S, 73°13′19.0″W	T, RH, G, U, Dir, R	2015	10 minutes
GT (lee)	350 m	51°07′01.6″S, 73°16′56.7″W	T, RH, U, Dir, R	2011	Daily, hourly

Tab. 2: Sensor types and accuracies of CE and NG (after Temme et al. 2020)

Variable	Sensor Name	Accuracy
T, RH	Campbell Scientific CS215	± 0.4 °C ± 4.0 %
U, Dir	Campbell Scientific Young 05108-45-L	± 0.3 m/s or 1 %
G	Campbell Scientific CS300	± 5.0 % of total daily radiation
RRR	Campbell Scientific Young 52202-L	± 3.0 % up to 50 mm/h ± 50.0 % local wind undercatch

mentioned AWSs are directly situated in a straight line crossing the mountain chain from west to east.

AWS Glacier Tyndall (GT) is located about 20 km southwards from NG. It delivers an additional insight in the conditions in the lee of the mountains. The station measures daily values of *T* and *R*. Since June 2018 *RH*, *U* and *Dir* have, additionally, been measured with records in an hourly resolution. The operating institution is the DGA.

The station on Cerro Tenerife (810 m a.s.l.), situated on Cerro Tenerife about 60 km southeastwards, delivers air pressure measurements as close to the study site as possible. Air pressure and air temperature measurements are used to determine air pressure at the four AWSs with the barometric height formula, which is necessary to calculate potential temperature that is used for the föhn identification.

In order to have a consistent time series of all four stations, the study period from 01 June 2018 – 31 May 2019 with overlapping data was chosen. The temporal resolution is hourly. To ensure correct values, data were quality checked and – if necessary – corrected. The datasets were searched for physically unreasonable values, outliers, consecutive identical values and periods of sensor freezing or radiative heating. For CE, it was known that the wind sensor was damaged over longer time. Wind direction and speed were excluded for these periods.

4.2 ERA5 reanalysis data

The WRF model is forced by ERA5 reanalysis data in 3-hourly timestep. The dataset is produced by the European Centre for Medium-Range Weather Forecasts (ECMWF). ERA5 provides a large number of atmospheric, land and oceanic climate variables in a high temporal and spatial resolution. Data is available on 137 vertical levels from the surface up to a height of 0.01 hPa, that are interpolated in the past-processed product to 37 pressure levels between 1000 hPa to 1 hPa. With a horizontal resolution of 31 km and an hourly output frequency, ERA5 is the most highly resolved globally available reanalysis dataset existing by now (Hersbach et al. 2019: 17ff.). ERA5 yields an overall improvement compared to previous versions and other reanalysis datasets, as has been demonstrated in various studies (e.g. Albergel et al. 2018; Olauson 2018).

4.3 Föhn Identification Algorithm

For the detection of föhn events, it is an established approach to use a Föhn Identification Algorithm that analyses meteorological processes during föhn from a phenomenological point of view (Vergeiner 2004: 66). Föhn Identification Algorithms have been applied in many locations, above all for the Alps (e.g. Drechsel/Mayr 2008, Plavcan et al. 2014, Vergeiner 2004), but also in the Southern Hemisphere like the Antarctic (e.g. Cape et al. 2015, Speirs et al. 2010, Turton et al. 2018, Wiesenekker et al. 2018), South Georgia (e.g. Bannister/King 2015) or South America (e.g. Palese/Cogliati 2015).

A new Föhn Identification Algorithm, taking into account the location-specific conditions of Patagonia, was developed (Temme et al. 2020). It is based on the detection algorithm used by Turton et al. 2018, Vergeiner 2004 and Palese/Cogliati 2015. The criteria used are: (i) changes in thermal state, (ii) changes in humidity, (iii) overflow of the mountain, and (iv) the potential temperature difference between the mountain and lee station. The latter avoids a false detection of thermally driven downslope flows during night where the potential temperature at the surface (on the lee side) would not reach or exceed the values of the mountain station (Drechsel/Mayr 2008: 217). This condition is only fulfilled if the vertical profile between the stations at the mountain and in the lee is dry adiabatically mixed, as it is during föhn events (Vergeiner 2004: 71).

The period, in which the changes in temperature and relative humidity were investigated, was set to 5 hours, which prevents false detection of periods with slowly adapting changes as well as short-lived changes in relative humidity or air temperature, which are too short for a föhn. The exact thresholds used in this algorithm are based on statistical values like in Turton et al. 2018, which makes the algorithm adaptable to different locations.

The two preconditions must be fulfilled:

1) $\Theta_{lee} + Ofs > \Theta_{ridge}$
   The potential temperature at the lee stations must exceed the potential temperature at the mountain station. However, to consider sensor accuracies, missing intercalibrations between the mountain and lee stations and uncertainties due to the extrapolation of potential temperature with data from a remote AWS, an offset (*Ofs* = 2.5 K) has been included.
2) 200°/220° < *Dir* < 320°
   Wind has to blow from the mountain. Thus, wind direction has to be between 220°– 320° and 200° – 320° for NG and GT, respectively. The sections were determined based on the topographical conditions around the stations.

Additionally, at least one of the following criteria needs to be met:

- RH decrease ≥ 14%/18% over 5 h: The relative humidity decrease over 5 h has to be equal or

higher than the 90th percentile of all 5-h humidity decreases at lee stations NG (14%) and GT (18%).
- RH < 10th percentile: Relative humidity is below the 10th percentile at lee stations.
- RH < 15th percentile & T increase ≥ 3.0 K / 3.5 K over 5 h: The relative humidity is below the 15th percentile (54% for NG, 49% for GT), and simultaneously, the air temperature increase is equal to or above the 90th percentile of all 5-h air temperature increases (3.0 K for NG, 3.5 K for GT).

This combination of criteria ensures that only föhn winds are identified as such. Modifying the thresholds softly did not produce a significant change in the number of identified days. This confirms the robustness of the algorithm.

4.4 Weather Research and Forecasting Model

For the high-resolution simulation of the atmosphere during a föhn event, the Weather Research and Forecasting (WRF) model, version 4.1 (Skamarock et al. 2019), was used. WRF is a numerical weather prediction and atmospheric simulation system designed for both research and operational applications. It provides the possibility to increase the resolution over an area of interest via grid nesting enabling high-resolution modelling. This way, large-scale phenomena are resolved in the parent domain whereas small-scale events are resolved in the nest.

The grid structure for this study is illustrated in Figure 3. The model was set up using one-way grid nesting over three domains centred at the SPI, increasing the horizontal resolution from 20 km in the parent domain (d01) to 4 km in d02 and to 1 km in d03. Due to the complex topography at the study site, the high resolution of the innermost domain is necessary to enable a meaningful simulation and analysis of the small-scale processes influencing a föhn event. To ensure that the simulation stays close to the meteorological input, nudging was activated in a 3-hourly time frame on domain d01. In the vertical, 50 levels were used.

The simulation length was set in a way to enable a model spin-up of 48 h and an analysis of the conditions one day before, during and one day after the föhn event, which takes place around 09 August 2018 (selection see section 5.1.2), determining a simulation period from 05 August 20:00 to 10 August 20:00 in local time (used further). According to the AWS measurements, the föhn event started on 09 August around 06:00 and ended around 20:00. The temporal resolution of the model output is increased from 6-hourly in the two outer domains to hourly in the innermost domain.

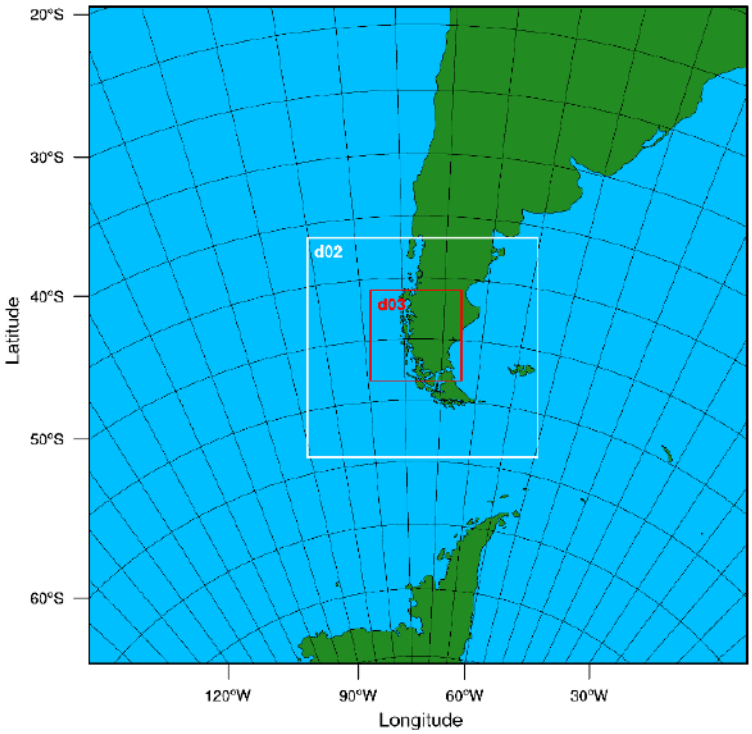

Fig. 3: Model domain configuration. The outermost domain d01 (black frame) has a horizontal resolution of 20 km. The inner domains d02 (white frame) and d03 (red frame) have a resolution of 4 km and 1 km, respectively.

Topography is provided by a high-resolution dataset with a resolution of about 500 m based on NASA Shuttle Radar Topography Mission (SRTM). Land use was determined by the Land Cover Classification System (LCCS) with a resolution of 300 m. To ensure proper results, especially concerning the glacier extents, a correction was applied to variables connected with landuse categories. Furthermore, snow-related variables had to be corrected to realistic values, like snow height to a maximum of 1 m.

In order to find the best set-up, 20 sensitivity runs were performed with a selection of parametrizations based on personal experience of the supervisors' research team and literature research. The best performing run was chosen based on qualitative and statistical evaluation. High-resolution modelling with WRF has been successfully used as an input for mass balance modelling (e.g. Schaefer et al. 2013; Schaefer et al. 2015) and for simulation of precipitation (e.g. Villarroel et al. 2013; Lenaerts et al. 2014; Sauter 2020) in Patagonia.

4.5 Evaluation design

In order to guarantee realistic simulations, WRF model surface variables were compared qualitatively

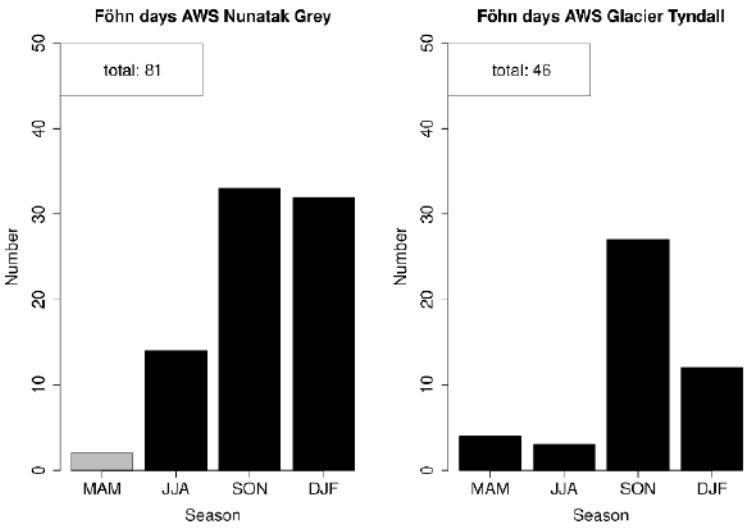

Fig. 4: Seasonal distribution of föhn days at NG and GT for March, April, May (MAM), June July, August (JJA), September, October, November (SON) and December, January, February (DJF). The respective total number is given in the top left corner. Note that MAM at NG (grey) lacks 2 months of data compared to GT.

and statistically with the AWS data considering *T*, *RH*, *G*, *U*, *Dir* and *R*. Attention must be paid regarding wind data because surface wind speed corresponds to 10 m above ground in the WRF model output but was measured at around 2 m above ground on the AWSs.

For the statistical evaluation of the agreement between model simulation and measurement, four statistical metrics are calculated: mean model bias (*MMB*) and Root Mean Square Error (*RMSE*) provide the absolute deviation between simulation and measurement, Pearson Correlation Coefficient (*r*) (derived from Wilks 2011) gives the relative agreement between model and observation regarding the variability of the variables, and Nash-Sutcliff efficiency (*NSE*) (introduced by Nash/Sutcliffe 1970) is a measure to evaluate the skill of the model to predict the observation.

5 Results & Discussion

5.1 Analysis of Föhn Days

In a first step, föhn events were detected during the study period of one year from 01 June 2018 to 31 May 2019. These events were investigated regarding their intensity, duration and suitability for a case study.

5.1.1 Amount and seasonal distribution of föhn events

In total, the algorithm identified 81 föhn days at NG and 46 föhn days at GT in the one-year study period (Figure 4). For NG, this means about two events per week. Personal experience on site can also confirm this frequency (Sauter, pers. comm.). Furthermore, föhn studies at South Georgia, which is located at similar latitudes, delivered a similar average annual amount of 87 events (Bannister/King 2015: 327). The results show that föhn events are likely to occur more frequently at NG than at GT. NG is located further from the ridge, more clearly in the lee of the mountains whereas GT is situated close to the ridge and at a higher altitude. Thus, the flow is stronger influenced by the mountainous terrain which is reflected in the more variable wind directions as well. Moreover, it is possible that the Föhn Identification Algorithm misses some of the föhn events at GT because the seasonal variation of the small-scale relative humidity and air temperature changes is stronger than at NG. As a consequence, it would be recommendable for future research to adapt the criteria values seasonally.

Despite the difference in frequency, the seasonal distribution of föhn days is similar for both stations. The highest occurrence of föhn events is in spring (September, October, November – SON) followed by summer (December, January, February – DJF). During these seasons, föhn events occur very frequently about 10–13 times a month at NG and 5–9 times a month at GT. This very high frequency of föhn events during spring and summer matches with the personal experiences on site that provide a guess of "several föhn events per week" (Sauter, pers. comm.). In autumn (March, April, May – MAM) and winter (June, July, August – JJA), the frequency is much lower. However, the number of föhn days in autumn at NG is not reliable because the station's measurements only reach up to 23 March. Thus, more than two months are missing in MAM compared to GT.

The seasonal distribution of föhn events matches with the stronger westerly winds during summer than winter (Garreaud et al. 2009). Due to the north-south orientation of the Andes, strengthened and more frequent westerlies can increase the frequency of föhn winds.

5.1.2 Determination of case study event

For the determination of the case study event, the identified föhn events were manually observed for the events with the highest signal of air temperature increase and relative humidity decrease and searched for events which occurred on both stations. In a second step, the synoptic situation at these days was analysed

to evaluate wind direction and strength as well as the upstream flow. Subsequently, seven föhn events with the strongest air temperature and relative humidity signal and an appropriate synoptic flow pattern were determined. For these events, the climatic situation at the AWSs was examined, which finally delivered one especially well pronounced case study föhn event, showing all the important föhn characteristics.

The case study föhn event took place on 09 August 2018. In Figure 5, the climatic conditions at the four AWSs are illustrated. The typical föhn characteristics can be observed very clearly. The event started on 09 August around 06:00 and ended around 20:00 lasting for about 14 hours. The conditions at the two lee stations are characterized by a moderate decrease in relative humidity that is more pronounced at GT. The air temperature increases strongly at both stations about 5°C within 2 to 3 hours. At the ridge (CE) and the windward station (FA), relative humidity increases and air temperatures decrease. This can be explained by an ascending of air masses upstream of the mountains, which usually provokes cooling. Therefore, condensation occurs and increases humidity up until (possibly) precipitation occurs. Hourly mean wind speeds clearly increase about 10 m/s. At NG, wind directions measure a stable northwestern flow pattern during the whole event (300°–320°). Considering the season, global radiation is relatively high with a maximum of nearly 400 W/m². At the lee stations, virtually no precipitation is measured, as expected. The small precipitation amount at GT could reflect a spill-over effect of the windward precipitation because the station is located close to the mountain ridge. Subsequently, a small eastward displacement of the föhn wall is sufficient to cause precipitation "spill" over the mountain ridge. Similar effects have been observed during föhn on the South-Island of New Zealand (e.g. McGowan/Sturman 1996). Stronger precipitation occurs on the windward side (FA).

5.2 Model Evaluation

For evaluation, WRF output is compared to measurements (Figure 6). *T* is best captured on the windward side. At the mountain plateau, *T* is overall well represented by the model. During the föhn event, the decreasing trend is visible like in the observation. In the lee, *T* is worse modelled. The first temperature rise on 08 August around noon is well captured by the model, but it misses the following decrease recorded by the observations. Subsequently, the model overestimates the temperatures before föhn onset and produces decreasing temperatures too early. Consequently, the föhn onset drawdown signals are produced temporally delayed. This also influences the statistical performance of both lee stations (Table 3). However, the model captures well the initial temperature rise as well as the end of the temperature decrease.

RH is, again, best reproduced on the windward side. At FA and CE, the absolute minimum is produced too early and slightly overestimated which influences the agreement in the following. Still, the *RH* rise during the föhn event is well captured in the model but starts and ends too early. At NG, the föhn-typical *RH* drop is modelled too early and too strong, causing that during the actual föhn event period an increase in humidity is produced. However, overlooking the timing, the initial signal of decreasing as well as the signal of increasing humidity at the end of the föhn event are captured well by the model. The same applies to the second lee station GT that performs better concerning the absolute *RH* values.

For *G*, reasonable measurements are only available at NG. The global radiation is underestimated by the model, whereas the variability is reproduced well which is confirmed by a strong correlation of 0.88 (Table 3). However, the low radiation values indicate problems for WRF to simulate cloud clearing associated with föhn conditions. However, the formation of lenticularis clouds in the lee is typical under föhn conditions (Stull 1988: 603).

Tab. 3: Statistics of model evaluation at each AWS. MMB and RMSE are in the respective variable's unit.

AWS	Statistic	T	RH	U	G
FA	MMB	-0.74	-6.64	-	-
	RMSE	1.73	19.94	-	-
	r	0.88	0.55	-	-
	NSE	0.66	0.19	-	-
CE	MMB	-1.88	-0.13	-	-
	RMSE	2.64	16.14	-	-
	r	0.63	0.22	-	-
	NSE	-1.22	-0.19	-	-
NG	MMB	-1.35	-1.79	2.84	16.15
	RMSE	3.22	16.74	5.31	57.29
	r	0.50	0.56	0.46	0.88
	NSE	-0.59	-1.90	-4.28	0.66
GT	MMB	-0.55	-0.85	0.85	-
	RMSE	2.64	13.55	2.75	-
	r	0.49	0.43	0.39	-
	NSE	0.06	-0.21	-0.34	-

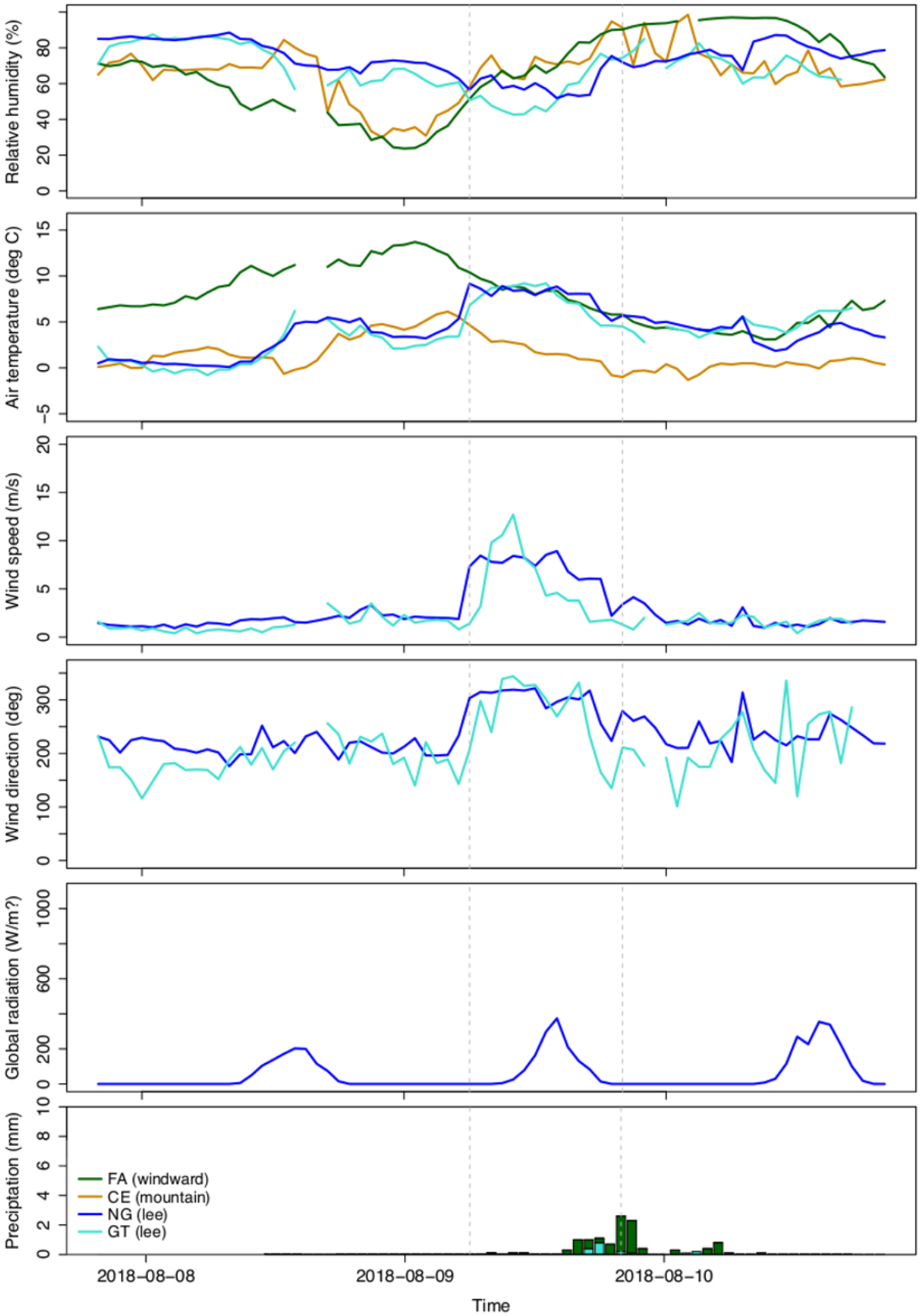

Fig. 5: Conditions at the AWSs during the case study föhn event. Dashed grey lines illustrate the beginning and end of the föhn event.

Wind speed and direction measurements are only available at the lee stations. Here, observations show a clear change from south-westerly to north-westerly flow together with a sudden increase in wind speeds at the begin of the föhn event. The increasing velocities are captured by the model at NG, but the timing is incorrect and the period of high wind speeds lasts too long. The U overestimation, which leads to high MMB and $RMSE$ (Table 3), is likely caused by the different height levels: While the wind sensor of the AWSs is installed at around 2 m above ground, the WRF model surface wind data is simulated at 10 m above ground. At GT, a clear increase in U is not visible.

Generally, the WRF model shows some weakness in simulating föhn over highly complex terrain in southern Patagonia, especially in the lee. A large and recurring issue is the timing offset between model and observation. In the observations, a signal of beginning föhn is occurring more than half a day before the actual event, retracting and afterwards the föhn sets on. The model does not capture this pattern and, subsequently, is temporally delayed during the

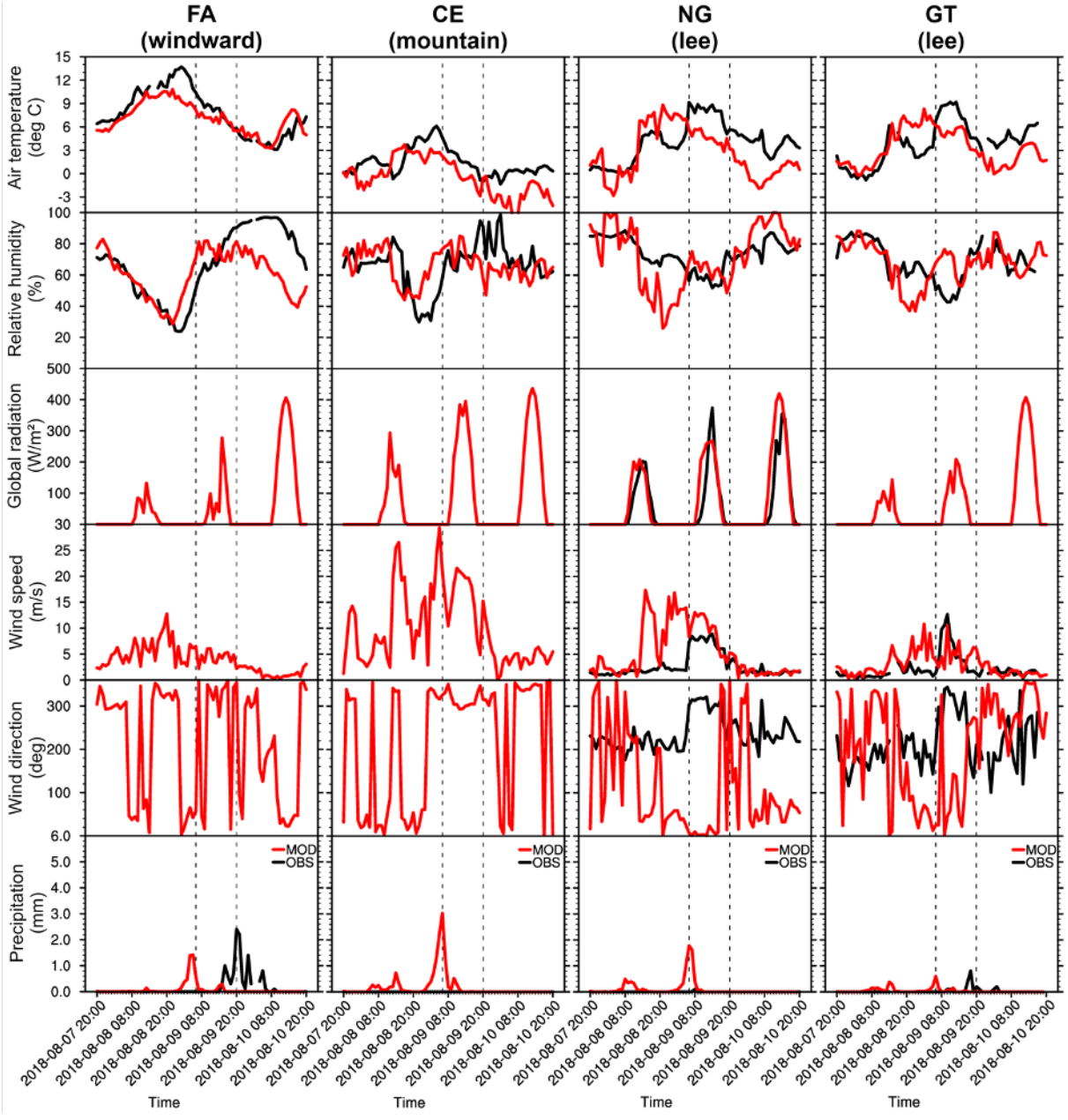

Fig. 6: Comparison of modelled (red line) meteorological surface variables of the respective closest grid cell with measurements (black line) at FA (windward), CE (mountain), NG (lee) and GT (lee). Dotted lines indicate the föhn period revealed by the AWS measurements. Note that wind speed corresponds to 10 m above ground in the model output but refers to around 2 m for the AWS data.

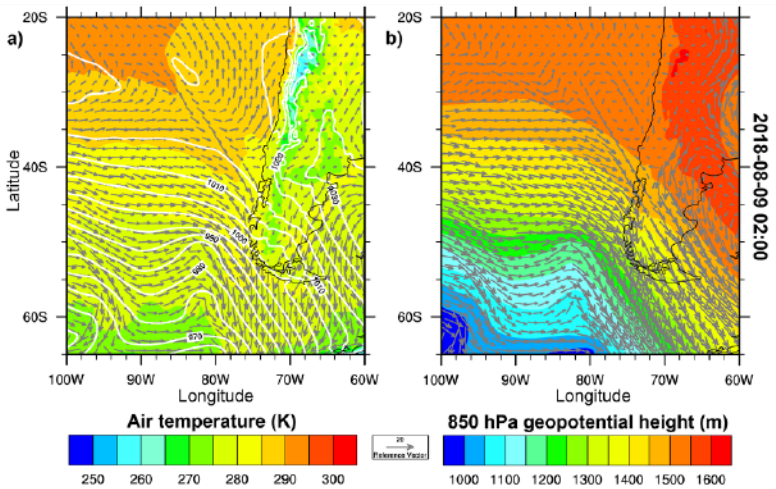

Fig. 7: Synoptic situation by a) 2 m air temperature (color scheme), sea level pressure (contours) and 10 m wind vectors (grey arrows) and b) 850 hPa geopotential height (color scheme) and wind vectors (arrows) at 2018-08-09 02:00.

whole study period. Similar conditions with timing issues were found in Turton et al. 2017. However, the typical föhn characteristics are captured by the model. This leads to the assumption that the simulation can be used for mesoscale analysis of the flow patterns during a föhn event. According to WRF, the föhn event is simulated between 08 August 18:00 and 09 August 18:00 with maximum föhn activity at 09 August 02:00. This period is used as the föhn event period in the following mesoscale analysis.

5.3 Mesoscale analysis of the case study föhn event

In order to give an encompassing insight over the processes that lead to föhn, and to investigate how the large-scale flow is reflected in the local-scale flow patterns, the analysis is performed on different scales. First, the general synoptic situation is analysed. Afterwards, vertical profiles of atmospheric variables upstream deliver information about the background flow. Finally, the mesoscale situation is investigated over the mountainous terrain. This way, the flow can be traced from the moment of approaching the continent until its arrival in the lee of the mountains.

5.3.1 Synoptic Situation

By föhn onset, a low-pressure system is situated in the south-east Pacific at the Patagonian coast and a high-pressure system over the continent (Figure 7). The intense pressure gradient between the systems causes extreme wind speeds. Subsequently, north-westerly flow from the southern subtropical Pacific is encountering the Andean chain. This flow mobilizes an advection of moist and warm air masses from the south-east Pacific with high velocities at the study site. The low-level flow is incapable of overflowing the mountain ridge and is deflected southwards which indicates the generation of a northern low-level jet along the Andes (Figure 7a). However, this only applies for the lowest few hundred meters as the upper-level flow maintains the north-westerly direction with high velocities (Figure 7b) and, thus, can overcome the mountains.

This synoptic situation with an intense pressure gradient due to the dipole of a low- and a high-pressure system inducing strong air flow perpendicular to the mountain range is typical for föhn situations, as well as the eventually formation of a low-level blocking (e.g. Zängl et al. 2004; Jang/Chun 2010; Mofidi et al. 2015).

5.3.2 Background flow characteristics

In order to analyse the upstream flow before it is modified by the mountains, the characteristics of the air masses approaching the Andes are investigated at an upstream location indicated in Figure 2. Therefore, the vertical profiles of wind speed (U), air (Ta), dewpoint (Td), equivalent potential (epT) and potential temperature (pT), and static stability before (T1), during (T2) and after (T3) the föhn event are presented in Figure 10. Static stability is given by the Brunt-Väisälä frequency (N), which returns the frequency at which an air parcel will oscillate when displaced vertically within a statically stable environment (Jackson et al. 2013: 122f.).

Horizontal wind speed increases strongly during the föhn event (Figure 8a). Before onset (T1), the velocities show an increase in the higher troposphere to tropopause indicating the prevalence of strong upper flow. With föhn onset, an increase in wind speed can be observed over all levels. These high values indicate that the approaching air flow will be able to overcome the Andes. In the lowest layer, extreme wind shear is apparent. At the peak of the event (T2), the layer with highest wind speeds drops down to around 1 km with slightly lower wind speeds overlying. Wind shear is still very intense in the lower troposphere with an increase of 10 m/s in less than 1 km. Extreme wind shear is a typical phenomenon developing in the upstream low-level stable layer during föhn. It has been reported during chinook storms in the Rocky Mountains and during föhn in the Alps (e.g. Klemp/Lilly 1975; Hoinka 1985). With föhn withdrawal (T3), the wind speeds decrease significantly.

Considering the four temperature variables (Figure 8b), it is visible that during the whole period the

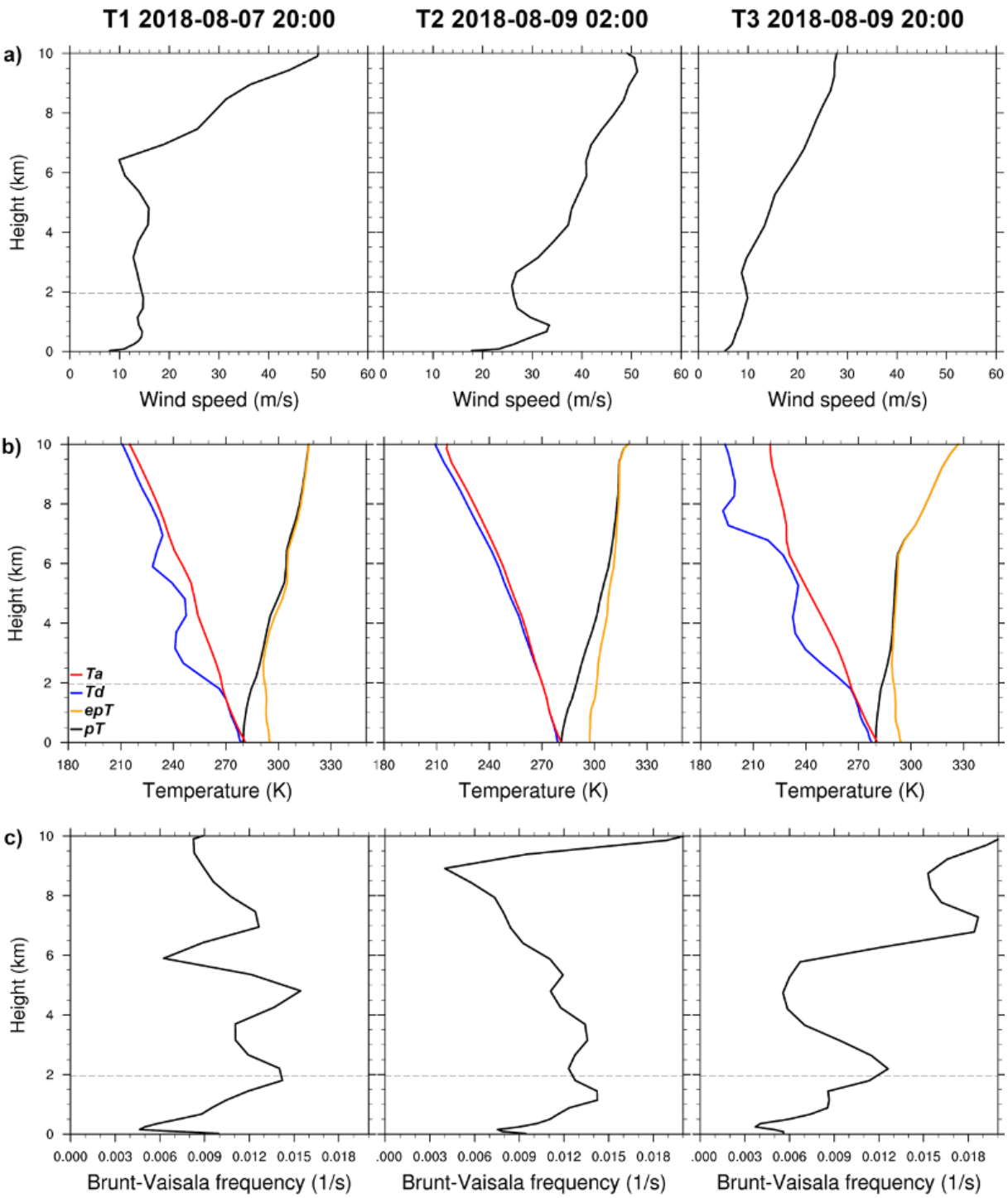

Fig. 8: Characteristics of the background flow upstream of the Andes at location indicated in Figure 3. Considered variables characterize the vertical structure of the undisturbed flow approaching the Andes and include measures for wind speed, temperature, moisture and stability. Dashed grey lines indicate mountain top level.

lower troposphere up to about 2 km is very moist. In the middle troposphere, the atmosphere is drier before (T1) and after (T3) the föhn event whereas with föhn ongoing (T2), the moist conditions reach into the higher troposphere. At the peak of the event (T2), the whole lower and mid-troposphere are highly saturated.

Equivalent potential temperature further delivers information about the stratification of the atmosphere as a measure of moist stability. The lower troposphere shows indifferent conditions before the event (T1), that change to potentially stable during the föhn (T2). Afterwards, conditions are going back towards indifferent or unstable.

The development of a potentially stable lower layer and the formation of an inversion layer just before and with föhn onset are common characteristics on the upwind side (Mofidi et al. 2015: 2499).

The dry static stability is described by the Brunt-Väisälä frequency *N* (Figure 8c). It shows that the troposphere is statically stably stratified over large parts. At the surface, the high values indicate strong stability which is overlain by an unstable layer that increases in stability with increasing height. Above, stratification is quite variable before the event with various very stable and more unstable layers (T1). With föhn onset, an extremely stable layer develops between 1.5 km to 2.5 km height with the maximum of stability around mountain top level. Together with the weak inversion visible in the potential temperature, the development of a high thermal stability is indicated. These characteristics are well known to provide an ideal environment for the generation of mountain waves (Hoinka 1985: 211ff.). During the event, the most stable layer sinks downwards to 1 km to 1.5 km height and is overlain by a layer of lower stability (T2). After the event (T3), the stratification is less stable up to a height of around 6 km with a stable layer around 2 km height. In other föhn studies very stable stratification in the lower troposphere together with a variability in *N* values with increasing height are observed similarly (e.g. Hoinka 1985; Jiang et al. 2005).

Overall, conditions during the föhn event show an extreme rise in wind speeds as well as strong wind shear in the lower troposphere. Additionally, the lower and mid-troposphere are stably stratified and moist during the event. This indicates the arrival of a warm and moist air mass with high wind speed at the moment of föhn onset. After its passage, the föhn event ends. These observations fit the considerations of the synoptic situation that also indicated an incident flow of warm and moist air masses from the south-east Pacific.

With *N*, the Froude number *Fr* can be calculated by $Fr = U/(Nh)$ with the mean horizontal wind speed *U* and the maximum mountain height *h* (Lin 2007: 125). It expresses the relationship between wind speed, stability and the height of the obstacle, and is a proven measure to classify the behaviour of an air parcel.

An air parcel with high wind speed and statically unstable stratification has advantage in flowing over the mountain barrier (Seluchi et al. 2003: 497). A $Fr < 1.0$ in the approaching air flow demonstrates subcritical flow indicating that the upstream flow is blocked and cannot overcome the obstacle whereas a $Fr > 1.0$ demonstrates supercritical flow indicating that the air flow can be lifted up to overflow the obstacle (Lin 2007: 33f.). Despite the stable stratification revealed by the Brunt-Väisälä frequency, *Fr* gives evidence that the approaching air masses are able to overflow the Andes, showing supercritical flow. According to Stull 1988, a *Fr* just above 1.0 reveals the highest wave motion with the possibility of rotor circulation near the surface. Furthermore, if sufficient moisture is present, standing lenticularis clouds can form along the crests of the waves (Stull 1988: 603). These preconditions are fulfilled just after the peak of the föhn event (around 2018-08-09 02:00).

5.3.3 Flow characteristics over the Andes

In order to trace the air flow from encountering the Andean chain to overflowing until flowing downwards in the lee, vertical cross sections of horizontal and vertical wind, potential and equivalent potential temperature, water vapor mixing ratio and cloud water mixing ratio are assessed. Cross sections are oriented along the mean flow axis during the föhn event with an angle of 310° and run through the location of NG (see Figure 2). Within the cross section, NG is situated downstream of the highest and most dominant mountain and directly upstream of another lower and smaller peak.

Before föhn onset (T1), wind speeds (Figure 9a) are low up to the higher troposphere where strong flow can be recognized. Small disturbances are present over the mountain ridge. During the event (T2), a faster air mass approaches the Andean chain. However, only weak updraft at the mountain barrier is indicated. In the direct lee of the highest peak, air masses are intensely accelerated to wind speeds up to 50 m/s. At the same location, wind vectors reveal downward motion indicating the local formation of a downward windstorm. Between the peaks and further downstream in the lee some small regions with low wind speeds are existent. Thus, the windstorm is not able to penetrate down to the foot of the mountain like it is often observed in studies with similar wind intensities (e.g. Mofidi et al. 2015). Wind vectors show strong vertical motion which indicates the formation of mountain waves all over the lower and mid-troposphere at a distance between the highest mountain peak and the lowest peak downstream. Acceleration is visible in the wave troughs whereas deceleration can be recognized in the wave crests. Close to the surface, some wind vectors in the lee also show reversed air flow. This feature indicates the formation of rotors (Jackson et al. 2013: 145ff.). After the föhn event (T3), wind speeds return to below 15 m/s in the lower troposphere and an intense upper-level air flow. Vertical disturbances over the mountain chain are still present but significantly reduced.

The vertical wind component is displayed together with equivalent potential temperature (Figure 9b). Positive wind values reveal upward motion while negative values reveal downward motion. Before

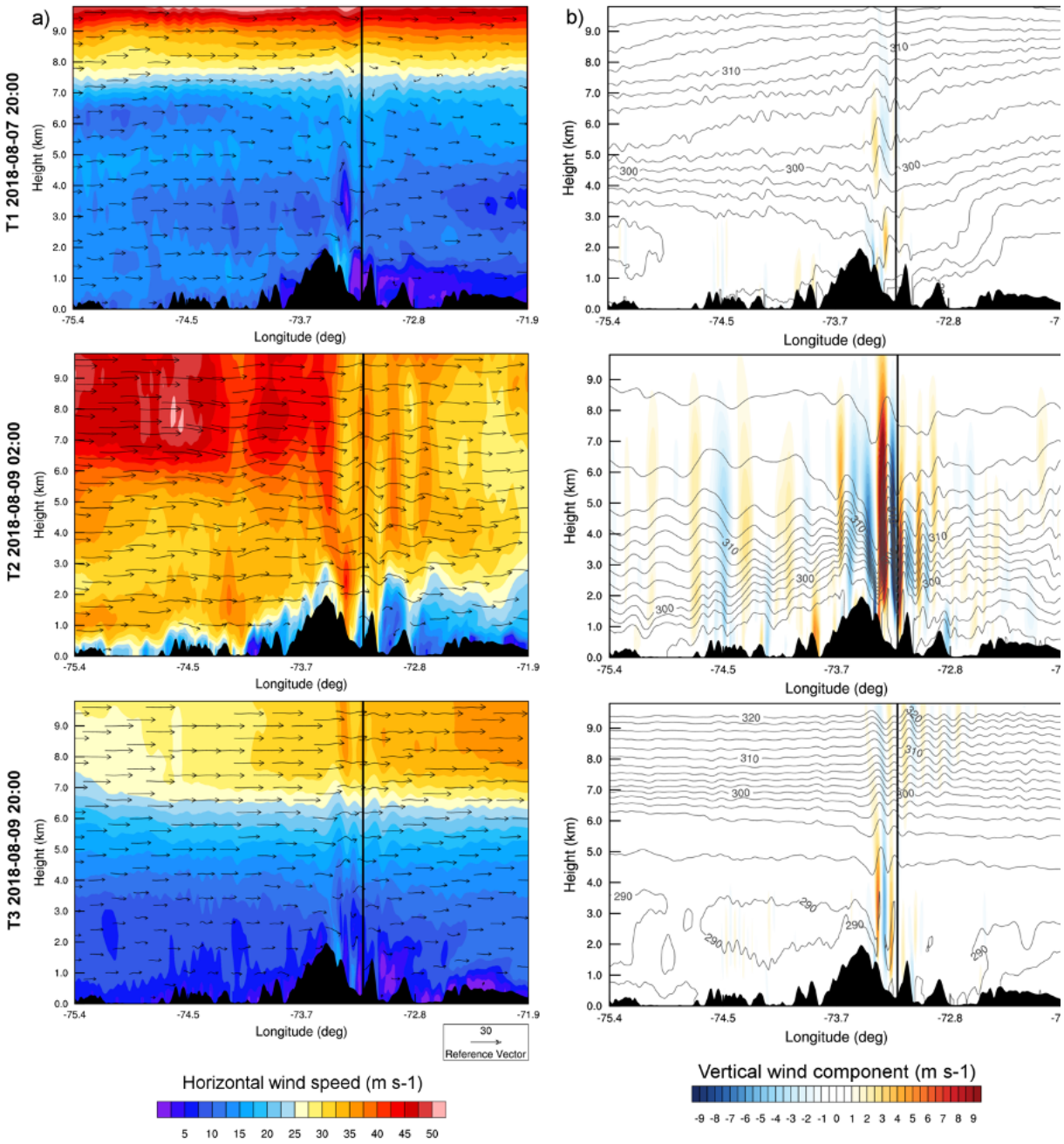

Fig. 9: Vertical cross section along main prevailing flow (310°) of a) horizontal wind speed (color scheme) together with wind vectors of along-cross-section and vertical component (arrows) and b) vertical wind component (color scheme) together with equivalent potential temperature (contour lines). Time steps are before (T1 2018-08-07), during (T2 2018-08-09 02:00) and after (T3 2018-08-09 20:00) the föhn event.

föhn onset (T1), virtually no vertical motion is visible. Equivalent potential temperature shows stably stratified conditions like seen in the vertical profiles of the upstream air flow (section 5.3.2). During the event (T2), the vertical wind component shows little updraft on the windward side. Extreme vertical motion is visible in the lee indicating the formation of mountain waves, which are extremely strong compared to other studies (e.g. Norte 2015, Mofidi et al. 2015, Zängl et al. 2004). Strongest mountain wave motion is between the highest mountain peak and the AWS location. Equivalent potential temperature demonstrates the same wave activity. Downward wind motion overlaps with troughs and upward wind motion with ridges in the *epT*-field. After the event (T3), vertical air motion has strongly decreased. However, residuals of the two most intense mountain waves continue to exist for some time.

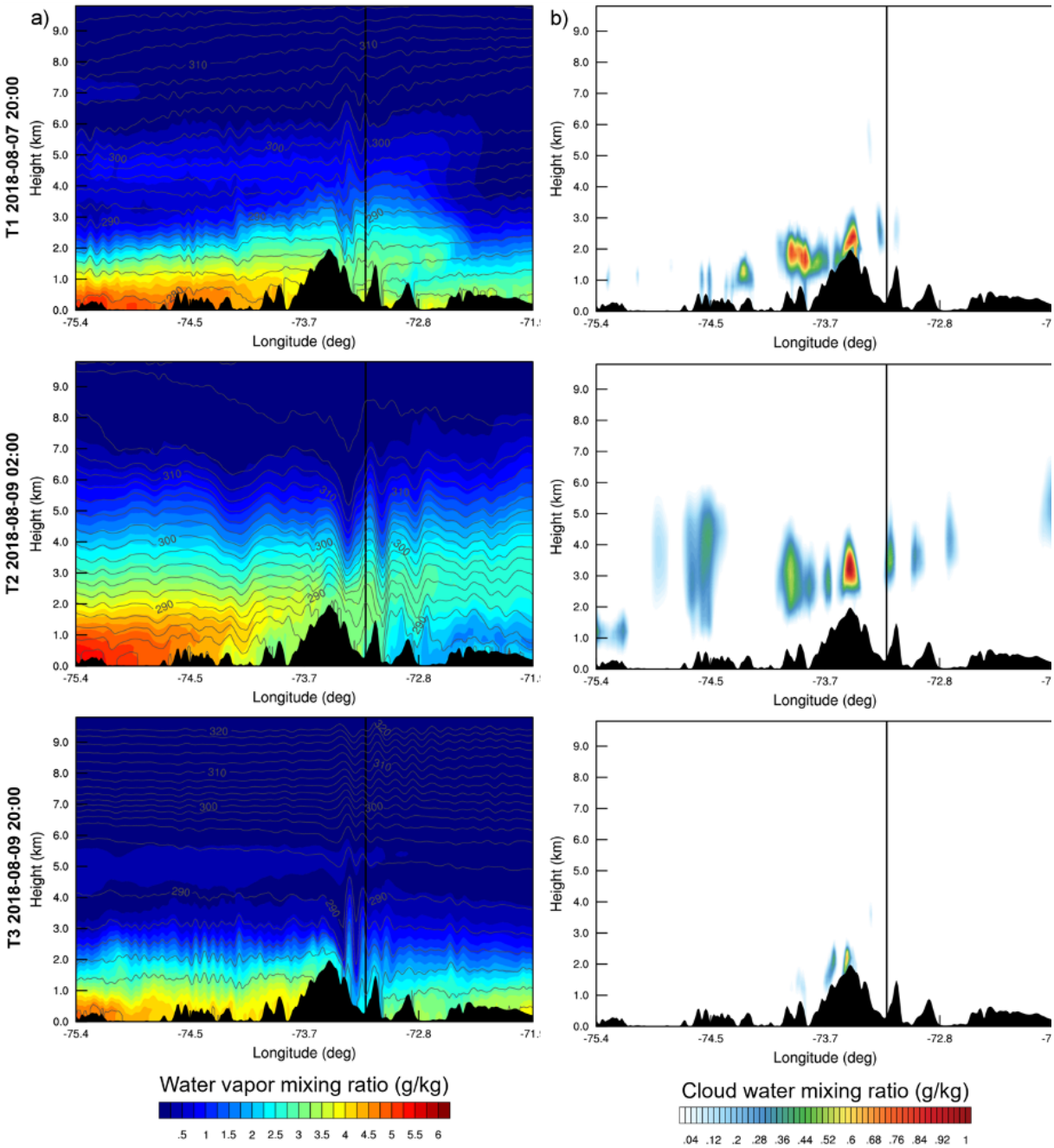

Fig. 10: Same as in Figure 9 for a) water vapor mixing ratio (color scheme) together with potential temperature (contour lines) and b) cloud water mixing ratio (color scheme).

As a measure of absolute moisture, water vapor mixing ratio is shown together with potential temperature (Figure 10a). Before föhn onset (T1), the moisture is increased in the lower troposphere up to around peak mountain height. Above, water vapor content is very low. Potential temperature increases with increasing height and shows small disturbances over the Andean chain. During the föhn event (T2), a deeper (up to a height of about 5 km), moist air mass approaches the study site. The moisture content of the lower troposphere increases on the windward side whereas in the lee it decreases. Furthermore, potential temperatures in the lee are several degrees higher than at the same altitude on the windward side due to the subsidence of potentially warmer air. Potential temperature shows intense mountain waves during the event. After the föhn event (T3), water vapor mixing ratio is very low in the whole troposphere above 2 km height. Lee wave motion remains and continues downward mixing of dry air

masses. Compared to other studies (e.g. Zängl et al. 2004; Mofidi et al. 2015; Norte 2015), pT indicates extreme mountain wave activity during the case study event. When the waves steepen and overturn, vertically proceeding isentropes occur which indicate the development of instability. This leads to non-linear flow associated with strong turbulence and wave-breaking (Mofidi et al. 2015: 2509 ff.). The extreme vertically oriented isentropes indicate that during the föhn event the flow regime is non-linear with wave-breaking existent, which can also lead to the formation of a surface-based hydraulic jump (Kirshbaum et al. 2018: 13).

To investigate cloud formation and activity, cloud water mixing ratio is considered (Figure 10b). Before the föhn event (T1), clouds exist in the lower troposphere above the mountain peaks, but in the lee skies are cloud-free. With the beginning of the event, several clouds form in the mid-troposphere above the mountain peak and in the direct lee (T2). In the lee, the formation of three small clouds is demonstrated which fit together with the wave crests, indicating the formation of standing lenticularis clouds (Stull 1988: 603). After föhn withdrawal (T3), the troposphere is cloud-free over the whole cross section area except for few small, low clouds directly above the mountain ridge. Above the AWS, the presumable formation of lenticularis clouds in the lee causes cloudy conditions during the event. This feature was also seen by the decreased global radiation in model evaluation (section 5.2).

Tracing the Froude number along the cross section (Figure 11) shows that before (T1) and after (T4) the event subcritical flow is prevailing all over, whereas during the event (T2 and T3) approaching air flow is supercritical until the obstacle is overcome. In the lee, around NG, *Fr* drops below 1.0 indicating an abrupt change to subcritical flow. This pattern is an indicator for the existence of a turbulent hydraulic jump (Durran 1990: 68; Lin 2007: 33 ff.; Kirshbaum et al. 2018: 13) and was observed similarly by Gohm et al. 2008.

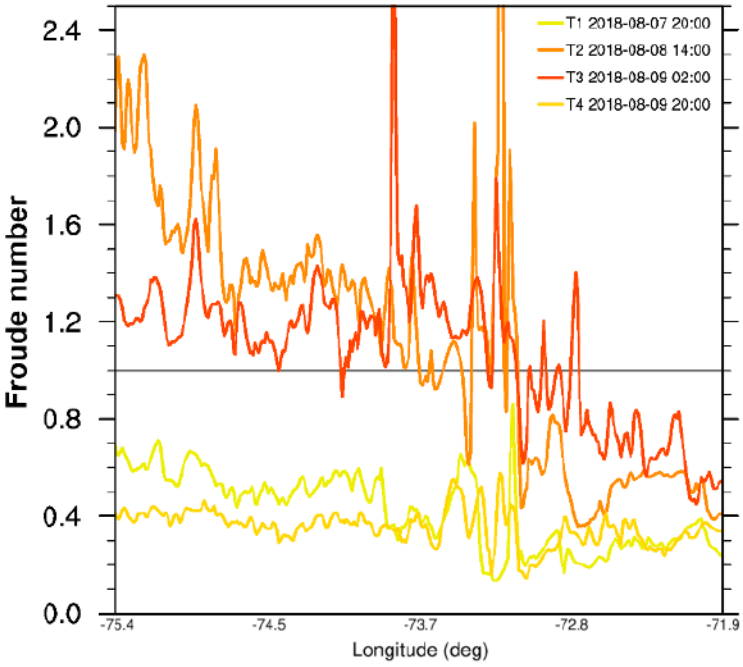

Fig. 11: Froude number along the cross section before (T1, light yellow), at onset (T2, orange), at maximum activity (T3, dark orange) and after the föhn event (T4, dark yellow). The horizontal black line indicates Fr = 1.0.

5.3.4 Summary of mesoscale analyses

The high-pressure system situated over the continent and low-pressure system west of the Patagonian coast force an intense pressure gradient causing strong north-westerly flow of warm and moist air masses, that initialize the föhn event. Before encountering the Andean chain, these air masses can be characterized as moist and very stable with high wind speeds. *Fr* reveals that the air flow is able to overflow the obstacle. Crossing the mountain ridge, strong winds are revealing and cause intense vertical air motion that features the development of large-amplitude mountain waves and a downslope windstorm. Furthermore, the atmospheric characteristics indicate the existence of wave-breaking and the possible formation of rotors and lenticularis clouds in the lee as well as a hydraulic jump. Studies have shown that severe local downslope winds and the formation of mountain-wave rotors are often associated with the existence of a hydraulic jump (e.g. Lin 2997, Durran 1990, Jackson et al. 2013).

Overall, these phenomena, the strength of the vertical air motion and the potential existence of a blocked low-level air mass suggest a non-linear flow regime. The weak upward flow on the windward side gives further evidence. Considering Serafin et al. 2018, the current conditions with the existence of a stable layer together with, after föhn onset, no formation of a low-level inversion above mountain-top level can cause large-amplitude hydrostatic waves favouring boundary-layer separation and turbulence (Serafin et al. 2018: 15 f.).

5.4 Case study föhn characteristics over the Southern Patagonian Icefield

WRF model output not only allows us to analyse the case study föhn event directly at the study site but additionally the larger area of the Southern Patagonian Icefield. Therefore, typical föhn

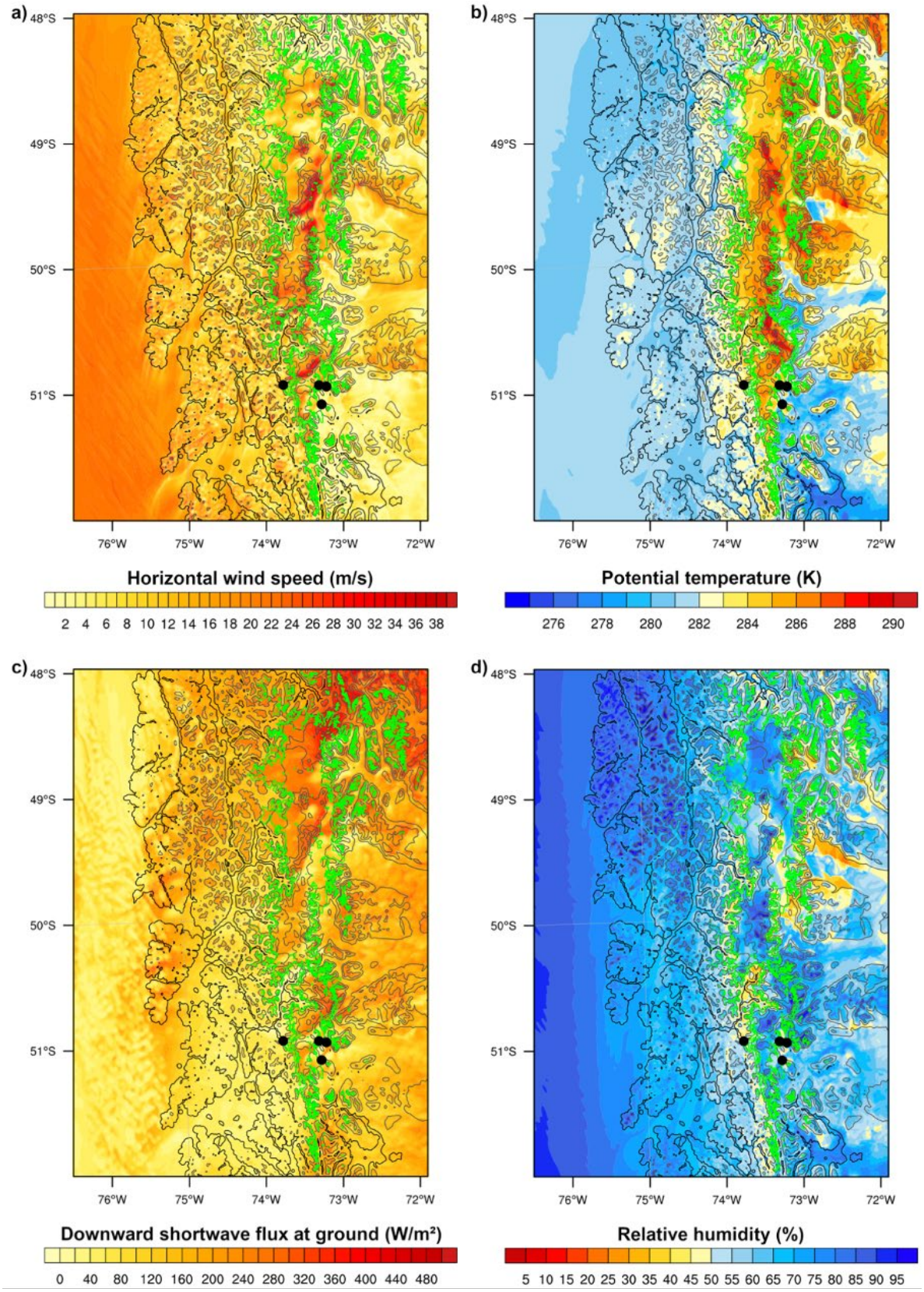

Fig. 12: Surface conditions of (a) the horizontal wind speed 10 m above ground, (b) potential temperature 2 m above ground, (c) downward shortwave flux at the ground, and (d) relative humidity 2 m above ground at 2018-08-08 18:00. Black dots indicate the AWS locations. The green contour outlines the glacierized area. Black/grey contours mark the terrain height in 500 m intervals (Temme et al. 2020).

characteristics are investigated over an area from 48°S – 52°S and 75.5°W – 72°W (Figure 2).

Horizontal wind speeds increase significantly over the Andean chain (Figure 12a). Regionally, velocity exceeds 40 m/s. Highest wind speeds in mountain lee are simulated around 49.3°S to 49.5°S and at the study site. However, it is noticeable that the strong winds are limited to the direct lee of the highest peaks and are not able to proceed further downstream.

Considering surface potential temperature (Figure 12b), it is expected that conditions are warmer in the lee compared to upstream during föhn. In the lee of the highest mountain peaks, a significant warming is evident, for example around 49°S to 50°S and at the study site. The SPI is affected by that as well, therefore, glaciated areas are facing air temperatures close to or even above the freezing point (not shown), which demonstrates the impact of föhn events on glacier ablation. The regions of most intense warming mainly overlap with the areas of highest wind speeds.

Shortwave radiation at the surface (Figure 12c) is especially enhanced in the northern part of the study site, in the lee and over parts of the mountains. Over the windward side, radiation is reduced indicating cloud formation in this area.

In the lee of the mountains, relative humidity is significantly lower compared to the windward side (Figure 12d). Strongest drying is visible in the lee of the study site and around 49.5°S. Over other parts of the area, regions with intense winds and warming do not exactly overlap with regions of strongest drying. Moister conditions around the mountain peaks, which would bring evidence for thermodynamic föhn with precipitation (Elvidge/Renfrew 2016: 456), are not simulated.

Overall, it can be shown that the case study föhn event extends not only over the study site, but also over the whole area of the SPI. However, regional differences exist leaving some regions less affected by the föhn than others. The most intense föhn activity and highest accordance with the conditions at the study site can be recognized around the highest mountain peaks. The question, if the study site is representative for the whole SPI concerning föhn events, cannot be answered clearly. Many characteristics like strengthening wind speeds, rising air temperatures or formation of mountain waves coincide with the study site. However, a decrease in moisture content in the lee cannot be recognized over large parts of the SPI. Considering this single föhn event, the study site is reflecting the föhn behaviour over large parts of the SPI fairly well. Nevertheless, in order to make a general statement, further research with analyses of several more föhn events would be necessary.

6 Conclusion

Föhn events are well-known in mountain ranges all over the world. However, research has so far not focused on southern Patagonia, which is predestined for föhn due to the mainly prevailing westerly flow perpendicular to the Andean mountain chain and the high wind speeds. This study has investigated the frequency and mesoscale processes of föhn events in southern Patagonia for a one-year study period from June 2018 to May 2019. Furthermore, the atmospheric processes during one case study event have been analysed and it was investigated how representative the study site is for the whole SPI.

The application of a Föhn Identification Algorithm to 10 months of the study period delivered 81 föhn days at the lee station NG. The seasonal distribution shows föhn events occurring most frequently in spring and summer, probably due to the higher wind speeds prevailing in these seasons. The findings of the föhn detection are overall consistent with personal experience on site and with other studies in a similar climatic environment (e.g. Bannister/King 2015). However, the results of the föhn identification could be improved by additional wind measurements at the ridge station and a seasonal variation of the algorithm's thresholds. From the identified föhn events, one especially clear and strong event (09 August 2018 between 06:00 and 20:00) was determined, which was simulated to analyse the mesoscale processes with WRF. The typical föhn characteristics in the lee, such as an increase in wind speed and air temperature and a decrease in relative humidity together with a westerly flow, can be observed.

An evaluation of the model performance demonstrated that WRF is capable of simulating föhn over highly complex terrain in southern Patagonia. The typical föhn characteristics, seen in the observations, are reproduced. However, the model shows several weaknesses, especially simulating the conditions in the lee. The most prominent issue is a timing offset, causing that the föhn event is simulated too early.

The synoptic situation inducing the föhn is characterized by a north-westerly flow of warm and moist air masses form the south-east Pacific with high wind speeds caused by a strong pressure gradient between a high-pressure system located over the Patagonian continent and a low-pressure system located southwest of the Patagonian coast. Crossing the Andes, strong winds cause intense vertical air motion in the lee of the mountains, forcing the development of large-amplitude mountain waves with the potential of wave-breaking. Furthermore, a downward windstorm in the direct lee of the mountains, the possible formation of rotors and the development

of standing lenticularis clouds in the wave crests are indicated. These flow patterns suggest that a non-linear flow regime prevails in a low-level stable layer, expressed by hydrostatic waves related to turbulence and boundary layer separation (Serafin et al. 2018: 15f.). Tracing the Froude number along the cross section indicates the formation of a hydraulic jump (Gohm et al. 2008: 34f.), providing evidence for the non-linear character.

It was demonstrated that the event extends over major parts of the SPI because many föhn characteristics, like wind patterns or the formation of mountain waves, coincide. Subsequently, it was shown that the case study föhn event reflects conditions over a large part of the SPI. However, based on a single event, a general statement about the representativity of föhn activity at the study site for the SPI cannot be made. Further analyses of several more föhn events would be necessary to do so.

Classifying föhn flow in southern Patagonia holds important potential for biogeographical, climatological and glaciological research. It is still not possible to give accurate estimates of precipitation amounts over the Patagonian icefields (Weidemann et al. 2018b; Sauter 2020). The leeside warming potentially influences glacier ablation (Norte 2015: 164). Due to the high frequency of föhn days identified in this study, a significant impact on the local climate is evident. Future research is desirable to improve knowledge about the influence of föhn on climatology, glaciology and biogeography in southern Patagonia.

Literature

Albergel, C.; Dutra, E.; Munier, S.; Calvet, J.-C.; Munoz-Sabater, J.; de Rosnay, P.; Bannister, G.; King, D. and J. 2015: Föhn winds on South Georgia and their impact on regional climate. Weather 70 (11): 324–329.

Braun, M.H.; Malz, P.; Sommer, C.; Farías-Barahona, D.; Sauter, T.; Casassa, G.; Soruco, A. Skvarca, P.; Seehaus, T.C. 2019: Constraining glacier elevation and mass changes in South America. Nature Climate Change 9 (2): 130–136.

Bravo, C.; Bozkurt, D.; Gonzalez-Reyes, Á.; Quincey, D.J.; Ross, A.N.; Farías-Barahona D.; Rojas, M. 2019: Assessing Snow Accumulation Patterns and Changes on the Patagonian Icefields. Frontiers in Environmental Science 7: 1–18.

Cape, M.R.; Vernet, M.; Skvarca, P.; Marinsek, S. Scambos, T. Domack, E. 2015: Foehn winds link climate-driven warming to ice shelf evolution in Antarctica. Journal of Geophysical Research: Atmospheres 120 (21): 11,037-11,057.

DGA. 2019: Inventario de Glaciares, https://www.arcgis.com/apps/View/index.html?appid=22f3177dc38d4e15ab84095e41d9c641, accessed 26 August 2019.

Drechsel, S.; Mayr, G.J. 2008: Objective Forecasting of Foehn Winds for a Subgrid-Scale Alpine Valley. Weather and Forecasting 23 (2): 205–218.

Durran, D.R. 1990: Mountain Waves and Downslope Winds. In: Banta, R.M.; Berri, G.; Blumen, W.; Carruthers, D.J.; Dalu, G.A.; Durran, D.R.; Egger, J.; Garratt, J.R.; Hanna, S.R.; Hunt, J.C.R.; Meroney, R.N.; Miller, W.; Neff, W.D.; Nicolini, M.; Paegle, J.; Pielke, R.A.; Smith, R.B.; Strimaitis, D.G.; Vukicevic, T.; Whiteman, C.D. (eds): Atmospheric Processes over Complex Terrain, Boston, MA. 59–81.

Elvidge, A.D.; Renfrew, I.A. 2016: The Causes of Foehn Warming in the Lee of Mountains. Bulletin of the American Meteorological Society 97 (3): 455–466.

Elvidge, A.D.; Renfrew, I.A.; King, J.C.; Orr, A.; Lachlan-Cope, T.A.; Weeks, M.; Gray, S.L. 2015: Foehn jets over the Larsen C Ice Shelf, Antarctica. Quarterly Journal of the Royal Meteorological Society 141 (688): 698–713.

Elvidge, A.D.; Kuipers Munneke, P.; King, J.C.; Renfrew, I.A.; Gilbert, E. 2020: Atmospheric drivers of melt on Larsen C Ice Shelf: Surface energy budget regimes and the impact of foehn. Journal of Geophysical Research: Atmosphere 125 (17): 1–25.

Garreaud, R. 2009: The Andes climate and weather. Advances in Geosciences 7: 1–9.

Garreaud, R.; Lopez, P.; Minvielle, M.; Rojas, M. 2013: Large-Scale Control on the Patagonian Climate. Journal of Climate 26 (1): 215–230.

Garreaud, R.D.; Vuille, M.; Compagnucci, R.; Marengo, J. 2009: Present-day South American climate. Palaeogeography, Palaeoclimatology, Palaeoecology 281 (3-4): 180–195.

Gohm, A.; Mayr, G.J.; Fix, A.; Giez, A. 2008: On the onset of bora and the formation of rotors and jumps near a mountain gap. Quarterly Journal of the Royal Meteorological Society 134: 21–46.

Hersbach, H.; Bell, W.; Berrisford, P.; Horányi, A.; Muñoz-Sabater, J.; Nicolas, J.; Radu, R.; Schepers, D.; Simmons, A.; Soci, C.; Dee, D. 2019: Global reanalysis: goodbye ERA-Interim, hello ERA5.

Hoinka, K.P. 1985: Observation of the airflow over the alps during a foehn event. Quarterly Journal of the Royal Meteorological Society 111 (467): 199–224.

Iacono, M.J.; Delamere, J.S.; Mlawer, E.J.; Shephard, M.W.; Clough, S.A.; Collins, W.D. 2008: Radiative forcing by long-lived greenhouse gases: Calculations with the AER radiative transfer models. Journal of Geophysical Research 113 (D13): 233.

Jackson, P.L.; Mayr, G.; Vosper, S. 2013: Dynamically-Driven Winds 55: 121–218.

Jang, W.; Chun, H.-Y. 2010: A numerical study on severe downslope windstorms occurred on 5 April 2005 at Gangneung and Yangyang, Korea. Asia-Pacific Journal of Atmospheric Sciences 46 (2): 155–172.

Jiang, Q.; Doyle, J.D.; Smith, R.B. 2005: Blocking, descent and gravity waves: Observations and modelling of a MAP northerly föhn event. Quarterly Journal of the Royal Meteorological Society 131 (606): 675–701.

Kain, J.S. 2004: The Kain-Fritsch Convective Parameterization: An Update. Journal of Applied Meteorology 43 (1): 170–181.

King, J.C.; Kirchgaessner, A.; Bevan, S.; Elvidge, A.D.; Kuipers Munneke, P.; Luckman, A.; Orr, A.; Renfrew, I.A.; van den Broeke, M.R. 2017: The Impact of Föhn Winds on Surface Energy Balance During the 2010–2011 Melt Season Over Larsen C Ice Shelf, Antarctica. Journal of Geophysical Research: Atmospheres 122 (22): 12,062-12,076.

Kirshbaum, D.; Adler, B.; Kalthoff, N.; Barthlott, C.; Serafin, S. 2018: Moist Orographic Convection: Physical

Mechanisms and Links to Surface-Exchange Processes. Atmosphere 9 (80): 1–26.

Klemp, J.B.; Lilly, D.R. 1975: The Dynamics of Wave-Induced Downslope Winds. Journal of the Atmospheric Sciences 32 (2): 320–339.

Lenaerts, J.T.M.; van den Broeke, M.R.; van Wessem, J.M.; van de Berg, W.J.; van Meijgaard, E.; van Ulft, L.H.; Schaefer, M. 2014: Extreme Precipitation and Climate Gradients in Patagonia Revealed by High-Resolution Regional Atmospheric Climate Modeling. Journal of Climate 27 (12): 4607–4621.

Lin, Y.-L. 2007: Mesoscale Dynamics. Cambridge.

McGowan, H.A.; Sturman, A.P. 1996: Regional and local scale characteristics of foehn wind events over the South Island of New Zealand. Meteorology and Atmospheric Physics 58 (1-4): 151–164.

Mofidi, A.; Soltanzadeh, I.; Yousefi, Y.; Zarrin, A.; Soltani, M.; Masoompour Samakosh, J.; Azizi, G.; Miller, S.T.K. 2015: Modeling the exceptional south Foehn event (Garmij) over the Alborz Mountains during the extreme forest fire of December 2005. Natural Hazards 75 (3): 2489–2518.

Morrison, H.; Thompson, G.; Tatarskii, V. 2009: Impact of Cloud Microphysics on the Development of Trailing Stratiform Precipitation in a Simulated Squall Line: Comparison of One- and Two-Moment Schemes. Monthly Weather Review 137 (3): 991–1007.

Nakanishi, M.; Niino, H. 2006: An Improved Mellor–Yamada Level-3 Model: Its Numerical Stability and Application to a Regional Prediction of Advection Fog. Boundary-Layer Meteorology 119 (2): 397–407.

Nash, J.E.; Sutcliffe, J.V. 1970: River flow forecasting through conceptual models part I – A discussion of principles. Journal of Hydrology 10 (3): 282–290.

Niu, G.-Y.; Yang, Z.-L.; Mitchell, K.E.; Chen, F.; Ek, M.B.; Barlage, M.; Kumar, A.; Manning, K.; Niyogi, D.; Rosero, E.; Tewari, M.; Xia, Y. 2011: The community Noah land surface model with multiparameterization options (Noah-MP): 1. Model description and evaluation with local-scale measurements. Journal of Geophysical Research 116 (D12): 1381.

Norte, F.A. 2015: Understanding and Forecasting Zonda Wind (Andean Foehn) in Argentina: A Review. Atmospheric and Climate Sciences 05: 163–193.

Norte, F.A.; Ulke, A.G.; Simonelli, S.C.; Viale, M. 2008: The severe zonda wind event of 11 July 2006 east of the Andes Cordillera (Argentine): a case study using the BRAMS model. Meteorology and Atmospheric Physics 102 (1-2): 1–14.

Olauson, J. 2018: ERA5: The new champion of wind power modelling? Renewable Energy 126: 322–331.

Palese, C.; Cogliati, M. 2015: Viento Zonda Norpatagónico en Neuquén. Parte I: Detecctión. 11 p.

Plavcan, D.; Mayr, G.J.; Zeileis, A. 2014: Automatic and Probabilistic Foehn Diagnosis with a Statistical Mixture Model. Journal of Applied Meteorology and Climatology 53 (3): 652–659.

Richner, H.; Hächler, P. 2012: Understanding and Forecasting Alpine Foehn 35: 219–260.

Rignot, E.; Rivera, A.; Casassa, G. 2003: Contribution of the Patagonia Icefields of South America to sea level rise. Science (New York, N.Y.) 302 (5644): 434–437.

Sauter, T. 2020: Revisiting extreme precipitation amounts over southern South America and implications for the Patagonian Icefields. Hydrology and Earth System Sciences 24: 2003–2016.

Schaefer, M.; Machguth, H.; Falvey, M.; Casassa, G. 2013: Modeling past and future surface mass balance of the Northern Patagonia Icefield. Journal of Geophysical Research: Earth Surface 118 (2): 571–588.

Schaefer, M.; Machguth, H.; Falvey, M.; Casassa, G.; Rignot, E. 2015: Quantifying mass balance processes on the Southern Patagonia Icefield. The Cryosphere 9 (1): 25–35.

Schär, C. 2002: Mesoscale Mountains and the Larger-Scale Atmospheric Dynamics. A Review. In: Pearce, R.P. (ed.): Meteorology at the millennium. International geophysics series v. 83, San Diego.

Schneider, C.; Glaser, M.; Kilian, R.; Santana, A.; Butorovic, N. Casassa, G. 2003: Weather Observations across the Southern Andes At 53°S. Physical Geography 24 (2): 97–119.

Seluchi, M.E.; Norte, F.A.; Satyamurty, P.; Chan Chou, S. 2003: Analysis of Three Situations of the Foehn Effect over the Andes (Zonda Wind) Using the Eta-CPTEC Regional Model. Weather and Forecasting 18: 481–501.

Serafin, S.; Adler, B.; Cuxart, J.; de Wekker, S.; Gohm, A.; Grisogono, B.; Kalthoff, N.; Kirshbaum, D.; Rotach, M.; Schmidli, J.; Stiperski, I.; Večenaj, Ž.; Zardi, D.; 2018: Exchange Processes in the Atmospheric Boundary Layer Over Mountainous Terrain. Atmosphere 9 (3): 102.

Skamarock, W.C.; Klemp, J.B.; Dudhia, J.; Gill, D.O.; Liu, Z.; Berner, J.; Wang, W.; Powers, J.G.; Duda, M.G.; Barker, D.M.; Huang, X.-Y. 2019: A Description of the Advanced Research WRF Model Version 4.

Smith, R.B.; Evans, J.P. 2007: Orographic Precipitation and Water Vapor Fractionation over the Southern Andes. Journal of Hydrometeorology 8 (1): 3–19.

Speirs, J.C.; Steinhoff, D.F.: McGowan, H.A.; Bromwich, D.H.; Monaghan, A.J. 2010: Foehn Winds in the McMurdo Dry Valleys, Antarctica: The Origin of Extreme Warming Events*. Journal of Climate 23 (13): 3577–3598.

Stull, R.B. 1988: An Introduction to Boundary Layer Meteorology. Dordrecht.

Turton, J.V. 2017: The Spatial and Temporal Distribution of Föhn Winds on the Larsen C Ice Shelf, Antarctica.

Turton, J.V.; Kirchgaessner, A.; Ross, A.N.; King, J.C. 2017: Does high-resolution modelling improve the spatial analysis of föhn flow over the Larsen C Ice Shelf? Weather 72 (7): 192–196.

Turton, J.V.; Kirchgaessner, A.; Ross, A.N.; King, J.C. 2018: The spatial distribution and temporal variability of föhn winds over the Larsen C ice shelf, Antarctica. Quarterly Journal of the Royal Meteorological Society 144 (713): 1169–1178.

UCAR. 2019: Weather Research and Forecasting Model, https://www.mmm.ucar.edu/weather-research-and-forecasting-model.

Vergeiner, J. 2004: South foehn studies and a new foehn classification scheme in the Wipp and Inn valley.

Viale, M.; Garreaud, R. 2015: Orographic effects of the subtropical and extratropical Andes on upwind precipitating clouds. Journal of Geophysical Research: Atmospheres 120 (10): 4962–4974.

Villarroel, C.; Carrasco, J.F.; Casassa, G.; Falvey, M. 2013: Modeling Near-Surface Air Temperature and Precipitation Using WRF with 5-km Resolution in the Northern Patagonia Icefield: A Pilot Simulation. International Journal of Geosciences 04 (08): 1193–1199.

Weidemann, S.S.; Sauter, T.; Kilian, R.; Steger, D.; Butorovic, N.; Schneider, C. 2018a: A 17-year Record of Meteorological Observations Across the Gran Campo

Nevado Ice Cap in Southern Patagonia, Chile, Related to Synoptic Weather Types and Climate Modes. Frontiers in Earth Science 6: 505.

Weidemann, S.S., T. Sauter, P. Malz, R. Jaña, J. Arigony-Neto, G. Casassa and C. Schneider (2018b): Glacier Mass Changes of Lake-Terminating Grey and Tyndall Glaciers at the Southern Patagonia Icefield Derived From Geodetic Observations and Energy and Mass Balance Modeling. Frontiers in Earth Science 6: 1–16.

Wiesenekker, J.; Kuipers Munneke, P.; van den Broeke, M.; Smeets, C. 2018: A Multidecadal Analysis of Föhn Winds over Larsen C Ice Shelf from a Combination of Observations and Modeling. Atmosphere 9 (5): 172.

Wilks, D. 2011: Statistical Methods in the Atmospheric Sciences. 3rd ed. Oxford. *World Meteorological Organization* (1992): International Meteorological Vocabulary. Genf.

Zängl, G.; Gohm, A.; Geier, G. 2004: South foehn in the Wipp Valley ? Innsbruck region: Numerical simulations of the 24 October 1999 case (MAP-IOP 10). Meteorology and Atmospheric Physics 86 (3-4): 213–243.

Kurzfassung:
Föhn-Ereignisse in Süd-Patagonien: Klimatologische Merkmale und prozess-basierte Modellierung

Gebirge haben einen wichtigen Einfluss auf das regionale Wetter und die klimatischen Bedingungen, indem sie die großräumige Strömung modifizieren. Ein typisches Phänomen, das im Lee von Gebirgsketten auftreten kann, sind Föhnereignisse. Durch die Orientierung der Anden orthogonal zur vorherrschenden westlichen Strömung ist Patagonien prädestiniert für Föhn. Diese Ereignisse können verschiedenste Bereiche beeinflussen, wie. Klimatologie, Glaziologie und Biogeographie.Die vorliegende Studie liefert eine erste Föhn-Klimatologie sowie ein Überblick über die involvierten mesoskaligen Prozesse. Beobachtungsdaten von vier Automatischen Wetterstationen, die in West-Ost Richtung um 51°S über das Gebirge verteilt liegen, werden verwendet, um Föhnereignisse zu ermitteln. Die Auswahl eines Ereignisses als Fall-Studie („case study event“) ermöglicht es, für das Untersuchungsgebiet sowie eine größere Region (48°S – 52°S, 75.5°W – 72°W), welche das Südliche Patagonische Eisfeld einschließt, die beteiligten mesoskaligen Prozesse hochaufgelöst (1 km) mit dem Atmosphärenmodell WRF zu simulieren.Die Ergebnisse zeigen eine Häufigkeit von mindestens 87 Föhnereignissen während des Untersuchungszeitraums von einem Jahr (Juni 2018 – Mai 2019), wobei höhere Föhnaktivität im Frühling und Sommer verzeichnet wird. Angetrieben wird das Ereignis von einem starken nord-westliches Anströmen warmer und feuchter Luftmassen. Das Auftreffen stabiler Luftmassen mit hoher Geschwindigkeit auf die Anden führt zu starker vertikaler Bewegung im Lee, also orographisch induzierten Wellen. Phänomene wie starke Abwinde im Lee und die Formation eines hydraulischen Sprungs deuten darauf hin, dass ein nicht-lineares Strömungsregime vorherrscht. Es zeigt sich, dass sich das Ereignis mit ähnlichen Charakteristika über weite Teile des Südlichen Patagonischen Eisfeldes erstreckt. Die enorme Häufigkeit von Föhnereignissen in Südpatagonien macht den Einfluss auf das lokale Klima deutlich.

Schlagwörter: **Patagonien, Föhn, WRF, numerische Modellierung, atmosphärische Prozesse**

Autorin: Franziska Temme, franziska.temme@fau.de; Thomas Mölg, thomas.moelg@fau.de; Jenny Turton, jenny.turton@fau.de, Institut für Geographie, FAU Erlangen-Nürnberg; Tobias Sauter, tobias.sauter@geo.hu-berlin.de, Institut für Geographie, HU Berlin.